JOURNAL OF PETROLOGY

Journal of Petrology, 2017, Vol. 58, No. 8, 1619–1644
doi: 10.1093/petrology/egx067
Advance Access Publication Date: 13 October 2017
Original Article

OXFORD

Pulses of Plagioclase-laden Magmas and Stratigraphic Evolution in the Upper Zone of the Bushveld Complex, South Africa

Qian Yuan[1,2], Olivier Namur[3,4], Lennart Alexander Fischer[3,5], Richard James Roberts[6], Xinbiao Lü[1]* and Bernard Charlier[2,3]

[1]Faculty of Earth Resources, China University of Geosciences, Wuhan 430074, China; [2]Department of Geology, University of Liège, 4000 Sart Tilman, Belgium; [3]Institut für Mineralogie, Leibniz Universität Hannover, 30167 Hannover, Germany; [4]Department of Earth and Environmental Sciences, KU Leuven, 3001 Leuven, Belgium; [5]School of Physical Sciences, University of Tasmania, Hobart, TAS 7001, Australia; [6]Department of Geology, University of Pretoria, Hatfield, Pretoria, 0002, South Africa

*Corresponding author. Telephone: +86–15972934906. E-mail: Lvxb_01@163.com

Received October 26, 2016; Accepted October 11, 2017

ABSTRACT

Cumulate rocks of the Upper Main Zone and Upper Zone (UUMZ) of the Bushveld Complex, South Africa, contain the world's major resources of Fe–Ti–V ± P, hosted in Ti-magnetite and apatite, and are commonly considered as having crystallized from the last major injection of magma into the magma chamber. In this study, we present the petrography, modal proportions, whole-rock major element chemistry (260 samples), electron microprobe data (~10 000 analyses for plagioclase, olivine, and pyroxene), and compiled analyses of Cr in magnetite (239 samples) for the UUMZ sampled over 2·1 km of the Bierkraal drill cores in the western limb of the Complex. The UUMZ section exhibits a broad normal fractionation trend upwards, but a series of reversals to more primitive anorthite contents in plagioclase, Mg# in pyroxenes and olivine, Cr in whole-rocks and Cr in magnetite separates are observed, accompanied by the appearance or disappearance of various minerals. Anorthosite or leucogabbro layers are closely linked to these reversals; the reversals in An % of plagioclase are used as boundaries to divide the UUMZ into 18 cycles. These cycles are interpreted as indications of magma chamber replenishment by plagioclase-laden magmas (up to 20 vol. % plagioclase) and are also marked by spikes in Cr content. In addition, abundant Fe–Ti oxide-bearing plagioclase-rich rocks are identified in the lower half of the UUMZ. These have crystallized from a hybrid melt produced by the mixing of a new plagioclase-bearing magma batch and the resident magma. Further crystallization of this hybrid liquid may lead to the formation of magnetite layers in the lower part of the UUMZ. The Bushveld UUMZ therefore grew by multiple emplacements of crystal-laden magmas coming from deep-seated chambers. Slow cooling in a shallow chamber explains the systematic bottom-up compositional evolution in the cumulate pile within individual cycles. The residual melt reached silicate liquid immiscibility soon after the saturation of apatite. Thereafter, segregation of conjugate Fe-rich and Si-rich melts and crystallization of the paired melts produces cumulates with a smooth upward decrease in Fe–Ti oxides, whereas plagioclase mode increases in each apatite-bearing cycle. A comparison of systematic geochemical analyses and a detailed lithological stratigraphy between the Bushveld limbs demonstrates the possible connectivity between the western and eastern Upper Zone but indicates notable differences from the Bellevue section of the northern limb.

Key words: layered intrusion; cumulate; cryptic layering; replenishment; anorthosite; magnetite layer; nelsonite; crystal mush; Bushveld Complex

INTRODUCTION

The Bushveld Complex in South Africa is the largest mafic layered intrusion on Earth, and is made up of five limbs, the northern, eastern, western, far western and southeastern limbs (Fig. 1), with an overall area of 65 000 km^2 (Cawthorn & Walraven, 1998; Cawthorn, 2015). The intrusion was emplaced at *c.* 2·06 Ga (Buick *et al.*, 2001; Zeh *et al.*, 2015) and hosts world-class deposits of magmatic V, Cr and platinum group element (PGE) ore (see Lee, 1996; Maier *et al.*, 2012). The Upper Zone and Upper Main Zone (UUMZ) are commonly considered as the crystallization products of the last major melt injection in the Bushveld magma chamber (Cawthorn *et al.*, 1991; VanTongeren & Mathez, 2013). The stratigraphy of the UUMZ evolves from gabbronorite to Fe–Ti-oxide gabbros with numerous magnetitite, nelsonite and anorthosite layers. The upward mineralogical and chemical evolution of cumulate rocks in the UUMZ was traditionally interpreted as resulting from a process of closed-system fractional crystallization (Wager & Brown, 1968; von Gruenewaldt, 1973; Molyneux, 1974). The generally constant Sr-isotopic composition of the ~2·1 km cumulate pile above the Pyroxenite Marker (PM) supports this hypothesis (Kruger *et al.*, 1987; Tegner *et al.*, 2006; VanTongeren *et al.*, 2010), although some recent studies have suggested that the UUMZ may have crystallized from several batches of magmas possibly with constant isotopic compositions (Ashwal *et al.*, 2005; Scoon & Mitchell, 2012). Tegner *et al.* (2006) documented several reversals in mineral and bulk-rock composition in the overall fractionation trend. Based on the hypothesis of crystallization of the UUMZ as a closed system, they interpreted these cycles as resulting from magma inversion related to double diffusive convection occurring after the crystallization of magnetite layers. An alternative model, in which the cycles were produced by pressure fluctuations in a crystallizing magma chamber, was proposed by Cawthorn & Ashwal (2009).

However, there is evidence that the Bushveld UUMZ chamber may not have been closed to magma input, and may have formed from the injection of numerous isotopically homogeneous magmas. Ashwal *et al.* (2005) documented large reversals in mineral compositions and geophysical parameters (magnetic susceptibility, bulk-rock density) in a column through the UUMZ, using systematic electron microprobe data for the main rock-forming minerals of the Bellevue drill cores in the northern limb, and attributed these to the influxes of new primitive magma. In the eastern limb at Roossenekal, Scoon & Mitchell (2012) observed that a continuous evolution of bulk-rock compositions is observed in only the uppermost part of the Upper Zone (UZ), and concluded that the lower cumulate sections were formed by crystallization of successive pulses of magma.

Development of silicate liquid immiscibility during crystallization of the UUMZ may have also contributed to the modal and mineralogical variability observed in the cumulate sequence, either on a large scale at the top of the UZ, as proposed by VanTongeren & Mathez (2012), or on a smaller scale in the upper third of the UUMZ, termed the UZc (Fischer *et al.*, 2016).

Magnetitites, the most noticeable characteristic of the UZ, have been investigated extensively in previous studies (Willemse, 1969*a*; Cawthorn & McCarthy, 1985; Reynolds, 1985*a*, 1985*b*; von Gruenewaldt *et al.*, 1985; Cawthorn & Molyneux, 1986; von Gruenewaldt, 1993; Tegner *et al.*, 2006; Scoon & Mitchell, 2012; Maier *et al.*, 2012), but there is no consensus on the origin of these monomineralic layers, either in the UUMZ or in other mafic layered intrusions. Comprehensive studies of the anorthosite layers in the UZ are lacking (Cawthorn & Ashwal, 2009), although such rocks commonly underlie or overlie magnetite layers (Tegner *et al.*, 2006; Cawthorn, 2015).

In this study, we present new whole-rock major element and mineral composition data for the 2·1 km thick section of the UUMZ sampled in the Bierkraal drill cores of the western limb (Fig. 1). Our close sample spacing allows us to assess carefully the succession of rock types and cumulus phases and the possible formation mechanisms for the UUMZ.

GEOLOGICAL SETTING

Regional geology

The Bushveld Complex includes several units: the ultramafic–mafic intrusive Rustenburg Layered Suite (RLS), the felsic Rashoop Granophyre Suite, and the Lebowa Granite Suite (SACS, 1980). The Complex is overlain by rhyolites of the Rooiberg Group and the associated Stavoren granophyres (Buchanan *et al.*, 1999, 2002, 2004), which may be related to a volcanic episode prior to the emplacement of the RLS (Eales & Cawthorn, 1996), or have been formed by fractional crystallization of the RLS magma (VanTongeren *et al.*, 2010, 2016; Mathez *et al.*, 2013). In this study we use the term Bushveld Complex to refer to the layered mafic and ultramafic cumulates in the RLS for simplicity.

The Bushveld Complex intruded into sediments of the Transvaal Sequence on the northern margin of the Kalahari Craton at *c.* 2·06 Ga and cooled in less than 1 Myr (Zeh *et al.*, 2015). A bottom-up stratigraphic subdivision into five sections (Marginal, Lower, Critical, Main and Upper Zones) has been used for a long time (Hall, 1932), although proposed boundaries have changed and may need reconsideration (Cawthorn, 2015). The Marginal Zone, as a result of contamination by komatiites (Barnes *et al.*, 2010; Wilson, 2012; Maier *et al.*, 2016), is dominated by heterogeneous noritic rocks forming the base of the Complex and varies laterally in thickness, reaching a maximum thickness of 750 m in the western limb and 350 m in the eastern limb (Vermaak, 1976; Engelbrecht, 1985; Wilson, 2012, 2015). Marginal Zone not even present in some areas. The Lower Zone is mainly composed of orthopyroxenite

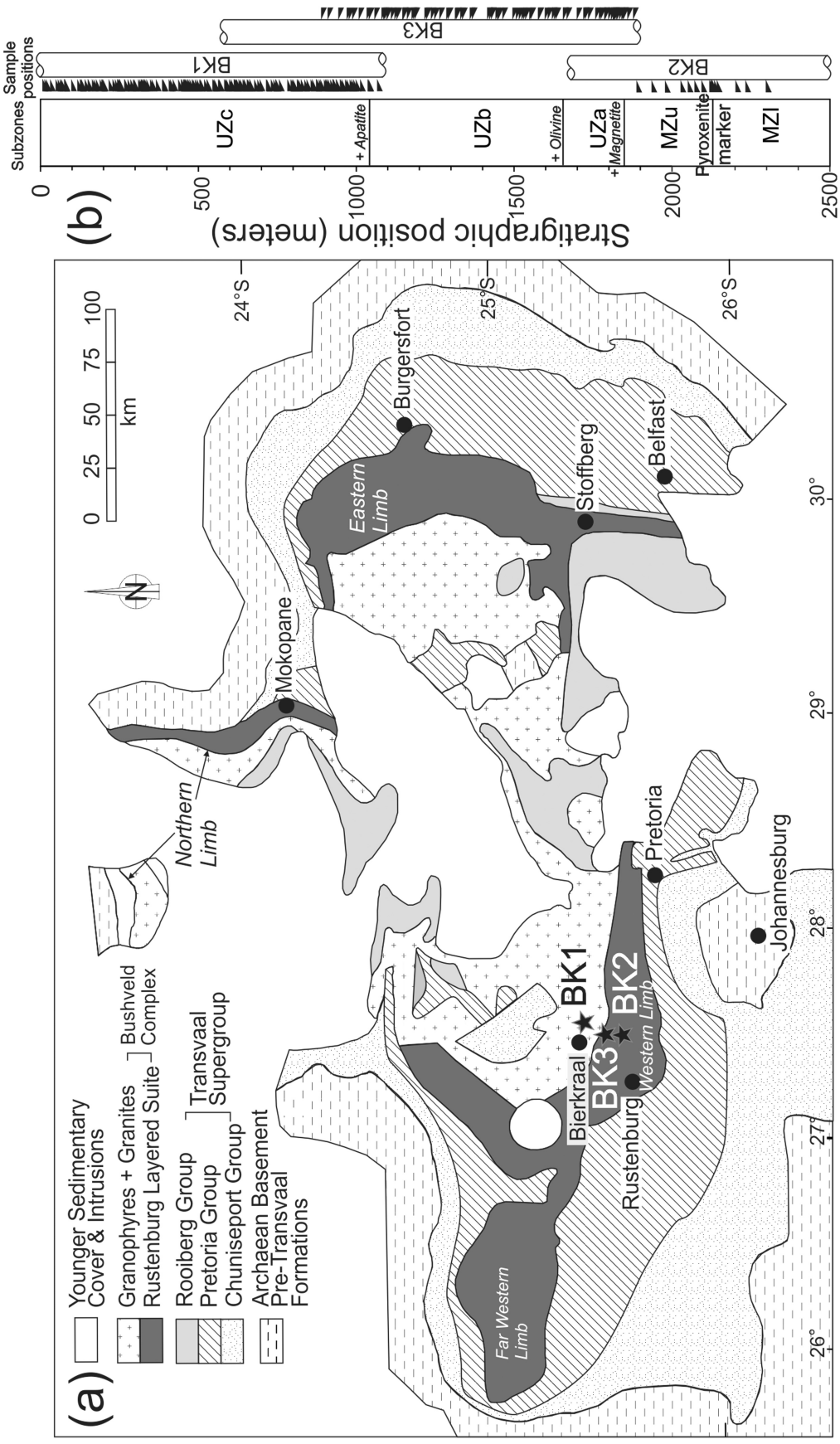

Fig. 1. (a) Simplified geological map of the Bushveld Complex showing the locations of BK1, BK2 and BK3 (modified after Barnes & Maier, 2002). (b) Schematic stratigraphic column of the upper part of the Bushveld Complex showing the locations of samples collected in drill cores BK1, BK2 and BK3. Subzones of the Upper Zone are defined by the appearance of cumulus titanomagnetite (UZa), olivine (UZb), and apatite (UZc). The Pyroxenite Marker separates the Upper Main Zone (MZu) from the Lower Main Zone (MZl).

and harzburgite interlayered with minor dunite. The Critical Zone has been divided into the pyroxenitic Lower and noritic Upper Critical Zones, both including abundant chromitite layers (Eales & Cawthorn, 1996). The Lower Main Zone (MZl) and Upper Main Zone (MZu) are dominated by norite and gabbronorite, respectively, and are separated in the western limb by a meter-thick pyroxenite layer considered to have crystallized from a hybrid melt during magma chamber replenishment (von Gruenewaldt, 1973; Molyneux, 1974; Cawthorn *et al.*, 1991; Mitchell, 1996; VanTongeren & Mathez, 2013).

Subdivision of the Upper and Upper Main Zones (UUMZ)

The Pyroxenite Marker (PM) is generally used to define the base of the MZu (Kruger *et al.*, 1987); this is represented by an apparent major and trace element reversal and a coincident change in whole-rock initial Sr isotopic composition (Sharpe, 1985; Kruger *et al.*, 1987; Cawthorn *et al.*, 1991, 2016). The PM has been documented in the eastern and possibly in the western limb (Cawthorn *et al.*, 1991; VanTongeren & Mathez, 2013), and a comparable stratigraphic unit of 4 m thick pyroxenite has been observed in the Bellevue drill core of the northern limb. However, the Bellevue pyroxenite cannot represent the same layer because of notable differences in the cumulus assemblage (Ashwal *et al.*, 2005). The total thickness of the UUMZ varies significantly. In Bierkraal drill cores of the western limb it is about 2·13 km (Fig. 2) (Tegner *et al.*, 2006). The eastern profile studied by von Gruenewaldt (1973) and Scoon & Mitchell (2012) is thicker (2·93 km) and made up of 630 m of the uppermost part of the MZu and 2300 m of the UZ, whereas the UUMZ section in the northern limb is thinner (1·59 km; Ashwal *et al.*, 2005).

Although various subdivisions have been proposed for the UUMZ (Willemse, 1969*a*, 1969*b*; von Gruenewaldt, 1973), in this study we use mineral appearances as boundaries for stratigraphic subdivision. In line with the previous study of Bierkraal cores (Tegner *et al.*, 2006), we choose the three-fold subdivision based on the first appearance of magnetite (UZa), olivine (UZb), and apatite (UZc) (von Gruenewaldt, 1973) (Figs 1 and 2).

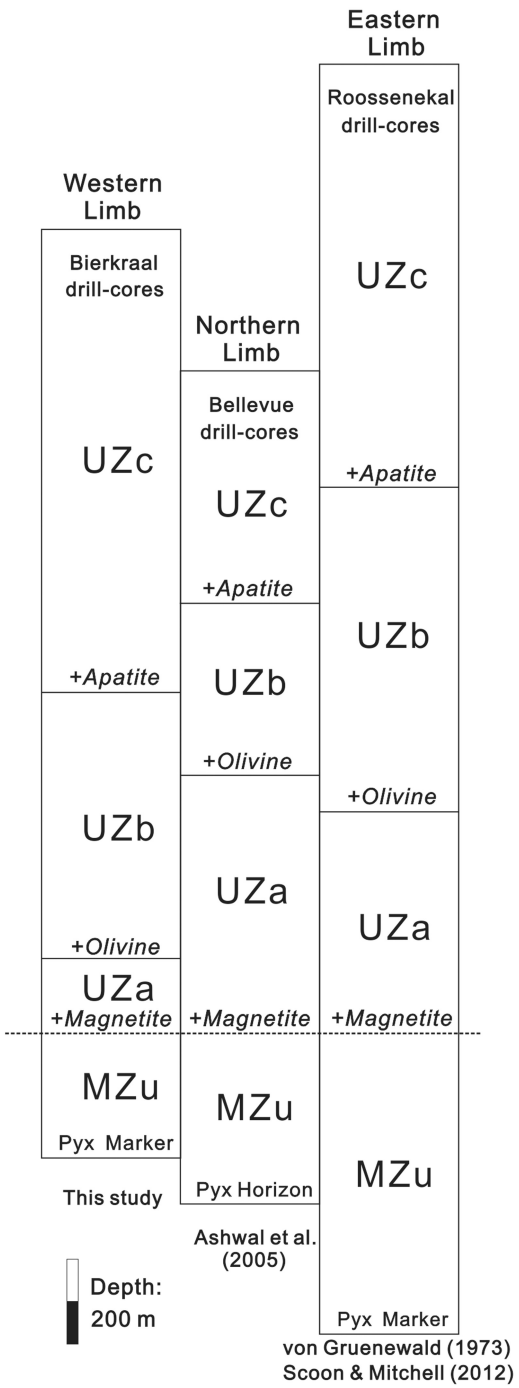

Fig. 2. Simplified stratigraphy of the Upper Main and Upper Zone in the western, northern and eastern limbs of the Bushveld Complex, based on the Bierkraal core (this study), the Bellevue core (Ashwal *et al.*, 2005) and the Roossenekal section (von Gruenewald, 1973; Scoon & Mitchell, 2012). Pyx Marker, Pyroxenite Marker, dominated by orthopyroxene; Pyx Horizon, dominated by high-Ca pyroxene.

SAMPLING

A continuous series of 260 samples was collected and analyzed from the Bierkraal drill cores to obtain a detailed section of the UUMZ with an average spacing between samples of less than 10 m (Fig. 1b). We also selected more closely spaced samples where lithological layering is pronounced. Only a few samples were collected from magnetite layers, as most of them have been sampled out in previous studies, but their stratigraphic locations have been reported to illustrate the lithological cycles. The samples come from three separate drill cores (BK1, 2 and 3), which were drilled and made available by the Council for Geoscience of South Africa (Walraven & Wolmarans, 1979). These cores have previously been studied in detail (Cawthorn & McCarthy, 1985; Reynolds, 1985*b*; Merkle & von Gruenewaldt, 1986; Kruger *et al.*, 1987; Cawthorn & Walsh, 1988; Cawthorn *et al.*, 1991; von Gruenewaldt,

1993; Tegner *et al.*, 2006), with a focus on the origin of the magnetitite layers, but so far no systematic integrated study based on detailed petrography, bulk-rock and mineral major element compositions has been presented. Stratigraphic correlation between the three drill cores is based on the position of the Main Magnetite Layer (MML) for BK2 and BK3, and the first appearance of apatite for BK1 and BK3 (Walraven & Wolmarans, 1979; Kruger *et al.*, 1987; Tegner *et al.*, 2006). The complete bottom-up section is therefore made up of the interval from 673 to 200 m depth in BK2 at the bottom, followed by the interval from 1420 to 550 m depth in BK3, and the top interval from 1600 to 415 m depth in BK1.

The true stratigraphic position and the distance between samples have been corrected, assuming that the core is vertical and the igneous layering dips at 24° NNE (Walraven & Wolmarans, 1979). Stratigraphic positions are also reported in meters with the '0 meter' reference level (411·8 m in BK1) marked by a diorite (Tegner *et al.*, 2006). The total stratigraphic section investigated in this study is 2128 m thick.

ANALYTICAL METHODS

Whole-rock compositions

Bulk-rock compositions were measured by X-ray fluorescence (XRF). All samples were carefully cleaned prior to crushing and milled in agate mortars. Major and trace elements (Cr and V) were determined using an ARL PERFORM-X 4200 at the University of Liège (Belgium). Ten major elements (Si, Ti, Al, Fe, Mn, Mg, Ca, Na, K, P) were measured on lithium tetra- and metaborate fused discs, with matrix correction following the Traill–Lachance algorithm. Trace elements (Cr and V) were measured on pressed powder pellets and the data were corrected for matrix effects by Compton peak monitoring. The major and trace element analyses are presented in Supplementary Table S1 (supplementary data are available for downloading at http://www.petrology.oxfordjournals.org).

Electron microprobe

The major element compositions of plagioclase were obtained with a JEOL JXA-8900R electron microprobe at the Institute of Mineralogy and Economic Geology at RWTH Aachen (Germany). The instrument was operated at an acceleration voltage of 15 kV, a probe current of 25 nA, and a beam diameter of 1–2 μm. The counting time for each element was 20 s. Natural and synthetic standards were used for calibration and the raw data were corrected with the standard ZAF correction.

The major element compositions of olivine and pyroxene were measured with a Cameca SX100 electron microprobe at the Institute of Mineralogy, Leibniz Universität Hannover (Germany). A 15 kV acceleration voltage was used for all analyses. Minerals were analyzed with a beam current of 15 nA and a focused beam (1 μm). The counting time for each element was 10 s. Raw data were corrected using standard PAP procedures (Pouchou & Pichoir, 1991). Standard materials for both electron microprobes include wollastonite (Si and Ca), albite (Na), orthoclase (K), and synthetic Al_2O_3, TiO_2, Fe_2O_3, MgO and Mn_3O_4. The results are presented in Supplementary Data Tables S2–S5.

Mineral mode determination

To determine mineral proportions we measured 98 samples with an FEI MLA 650 scanning electron microscope (SEM) at the University of Tasmania, Australia, using the XMOD protocol (X-ray modal). We analyzed ~25 000 points on a 20 mm × 10 mm representative area for each sample. The obtained energy-dispersive spectrometry (EDX) spectra were recorded and compared with a handmade mineral reference spectra database made with the Mineral Liberation Analysis (MLA) software package v3.1. When matched, single point analyses were assigned to a specific mineral. The results for mineral modes are listed in Supplementary Data Table S6. For the same rocks, we also calculated normative mineral modes using the CIPW norm. Because of the good correlation between CIPW norm calculations and MLA scanning for plagioclase and Fe–Ti oxides (Supplementary Data Figs S1 and S2), we used the CIPW norm to calculate mineral modes of these phases for the whole set of 260 rocks.

PETROGRAPHY AND MODAL PROPORTIONS

Petrography

The UUMZ is dominated by layered gabbronorite in MZu (Fig. 3a), magnetite gabbronorite (± olivine) in UZa and UZb (Fig. 3b and c), and magnetite gabbros, magnetite troctolite (Fig. 3d and e) and some ferrodiorite in UZc (Fig. 3f). A number of anorthosite layers, as well as Fe–Ti oxide-bearing plagioclase-rich samples [pmi-C following the nomenclature of Irvine (1982)] were also recognized (Fig. 4). Anorthosites generally have a few poikilitic high-Ca pyroxenes (Fig. 4a), which locally show some amphibolization. The pmi-C samples contain more than 70 vol. % subhedral to euhedral plagioclase with about 10 vol. % Fe–Ti oxides and a few irregularly distributed high-Ca pyroxene crystals (Fig. 4b). In addition to these dominant rock types, intermittent magnetite–ilmenite ± apatite-rich rocks are identified. The magnetite layers are largely dominated by massive polycrystalline Fe–Ti oxide aggregates (Ti-magnetite + ilmenite) and minor euhedral plagioclase with few interstitial mafic silicate minerals (Fig. 4c). Nelsonites are similar to magnetite layers but with plenty of apatite (Fig. 4d). The locations of these rocks in the Bierkraal core are shown in Fig. 5 and listed in Table 1.

Abundant anorthositic rocks occur in UUMZ and can be broadly divided into two types: anorthosite and pmi-C rocks (Fig. 4). Anorthosite contains more than 90% plagioclase, with the plagioclase usually containing

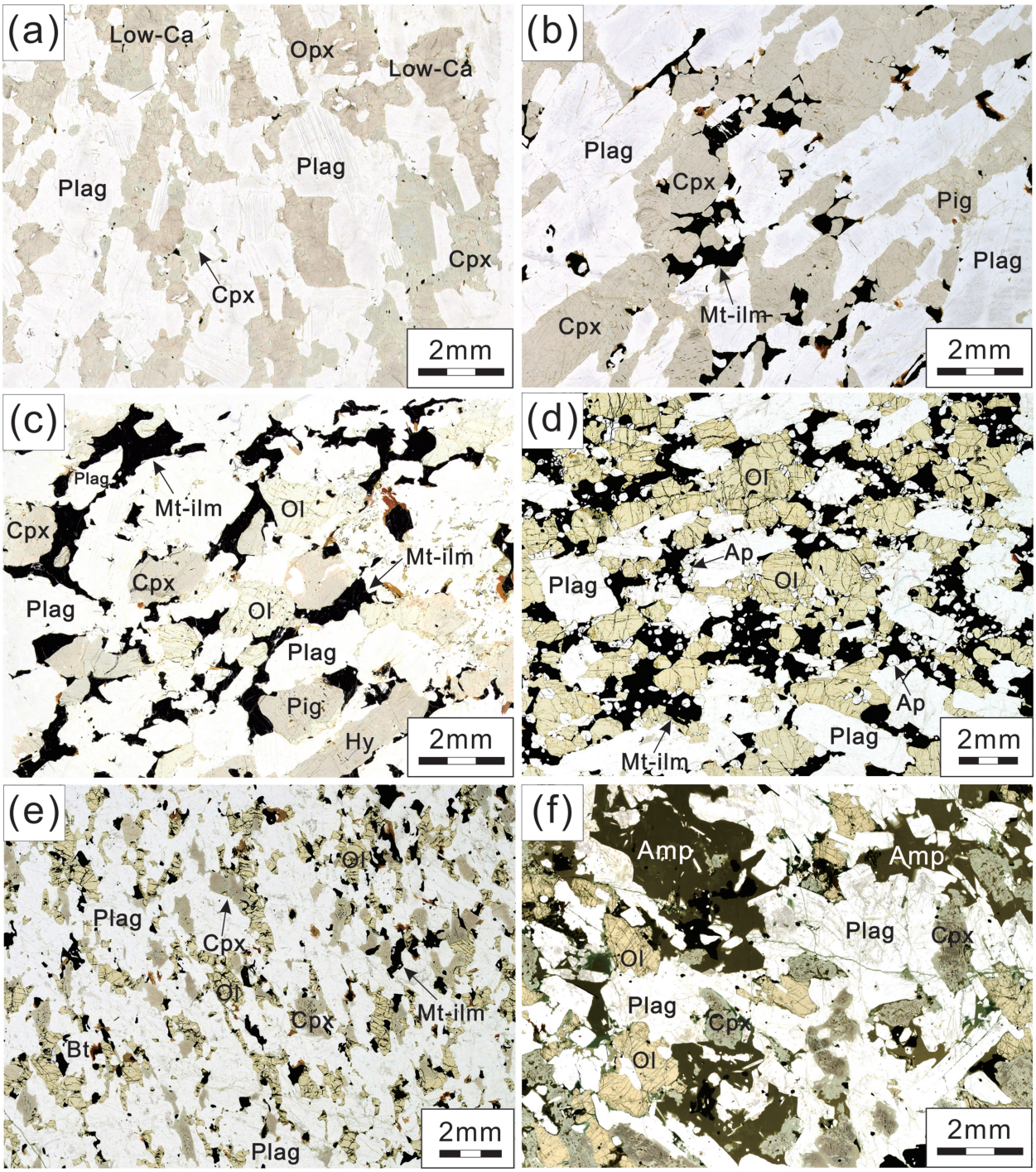

Fig. 3. Representative photomicrographs showing the main cumulus assemblages of rocks from the UUMZ of the Bushveld Complex. (a) Gabbronorite from the Upper Main Zone, containing abundant euhedral to subhedral tabular plagioclase and subhedral high-Ca pyroxene and some anhedral low-Ca pyroxene (sample 3w1399.6, MZu). (b) Magnetite gabbronorite dominated by large lath-shaped plagioclase and euhedral to subhedral high-Ca pyroxene with a few low-Ca pyroxene crystals; the appearance of Fe–Ti oxides should be noted (sample 3w1321.3, UZa). (c) Magnetite olivine gabbronorite containing large subhedral olivine, abundant nearly equiaxial shape high-Ca and low-Ca pyroxene, and lath-shaped grains of plagioclase and some anhedral Fe–Ti oxides. It should be noted that two kinds of low-Ca pyroxene appear: hypersthene as large elongated grains and inverted pigeonite as subhedral crystals (sample 3w1096.9, UZb). (d) Magnetite troctolite containing large grains of euhedral plagioclase and subhedral olivine and Fe–Ti oxides enclosing rounded grains of apatite. High-Ca pyroxene is absent (sample 1w1074, UZc). (e) Magnetite olivine gabbro containing abundant subhedral high-Ca pyroxene, lath-shaped plagioclase and some olivine. The well-defined magmatic lamination displayed by plagioclase should be noted (sample 1w1285.7, UZc). (f) Ferrodiorite at the top of UUMZ, with large subhedral to anhedral amphibole and subhedral plagioclase; olivine is sub-rounded and high-Ca pyroxene locally shows moderate alteration and has a close relationship with amphibole (sample 1w497.44, UZc). Plag, plagioclase; Cpx, high-Ca pyroxene; Opx, low-Ca pyroxene; Hy, hypersthene; Pig, inverted pigeonite; Mt-ilm, Fe–Ti oxides; Ol, olivine; Ap, apatite; Bt, biotite; Amp, amphibole.

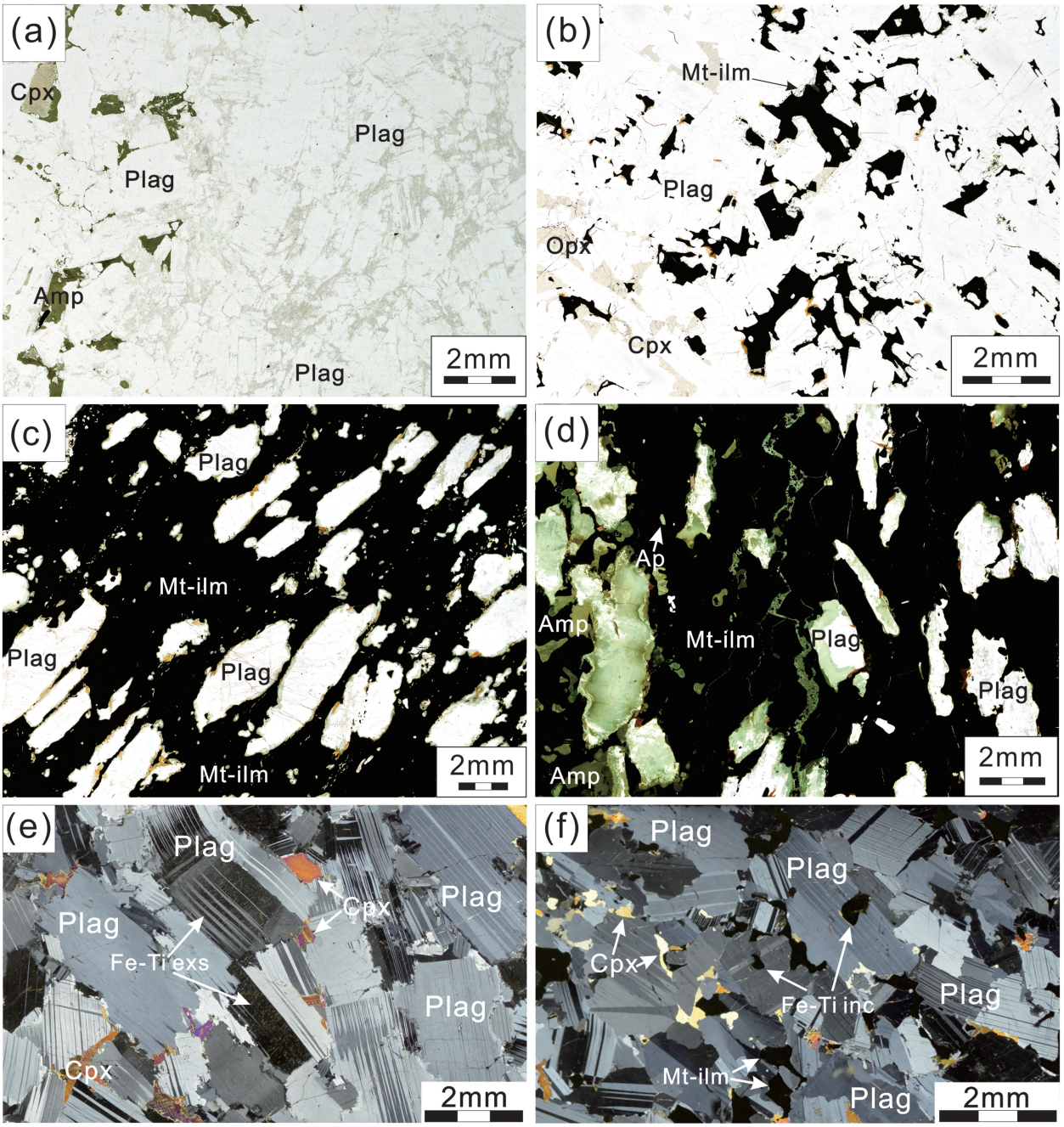

Fig. 4. Photomicrographs showing the textures in monomineralic rocks from the UUMZ of the Bushveld Complex. (a) Anorthosite with the right half of the image showing the partially molten texture and the left part a similar texture of plagioclase with some interstitial high-Ca pyroxene and amphibole. The amphibole rims on high-Ca pyroxene suggest that the amphibole may have been formed by alteration of high-Ca pyroxene (sample 1w830.6, UZc). (b) pmi-C sample dominated by large subhedral plagioclase and some irregular aggregates of Fe–Ti, with a few unequally distributed high-Ca pyroxene crystals (sample 3w1342.6, UZa). (c) Magnetitite containing abundant oriented lath-shaped plagioclase crystals and large aggregates of Fe–Ti oxides; some small plagioclase inclusions within Fe–Ti oxides and a few olivine grains intergrown with Fe–Ti oxides are observed (MML, sample 1w1343, UZc). (d) Nelsonite sample with abundant Fe–Ti oxides, euhedral apatite and some euhedral to subhedral plagioclase. Amphibolization masks some small apatite crystals (sample 1w1108, UZc). (e) Anorthosite from 3w1380.7; the serrated boundaries between the large plagioclase and abundant Fe–Ti oxide exsolution should be noted. (f) pmi-C of 3w1369.9, which has the earliest cumulate Fe–Ti oxides in the sample set; interstitial high-Ca pyroxene and subhedral Fe–Ti oxides within large plagioclase should be noted. Plag, plagioclase; Cpx, high-Ca pyroxene; Mt-ilm, Fe–Ti oxides; Fe–Ti inc, Fe–Ti inclusions; Fe–Ti exs, Fe–Ti exsolutions; Ap, apatite; Amp, amphibole.

abundant needle-like Fe–Ti oxide exsolutions. The boundary between the plagioclases is often slightly jagged or poorly defined, possibly owing to alteration or post-solidification modification (Fig. 4e). Compared with anorthosite, pmi-C rocks are characterized by more abundant Fe–Ti oxides and some interstitial high-Ca pyroxenes (Fig. 4f). Fe–Ti oxides can occur either as individual cumulate phases or as subhedral inclusions

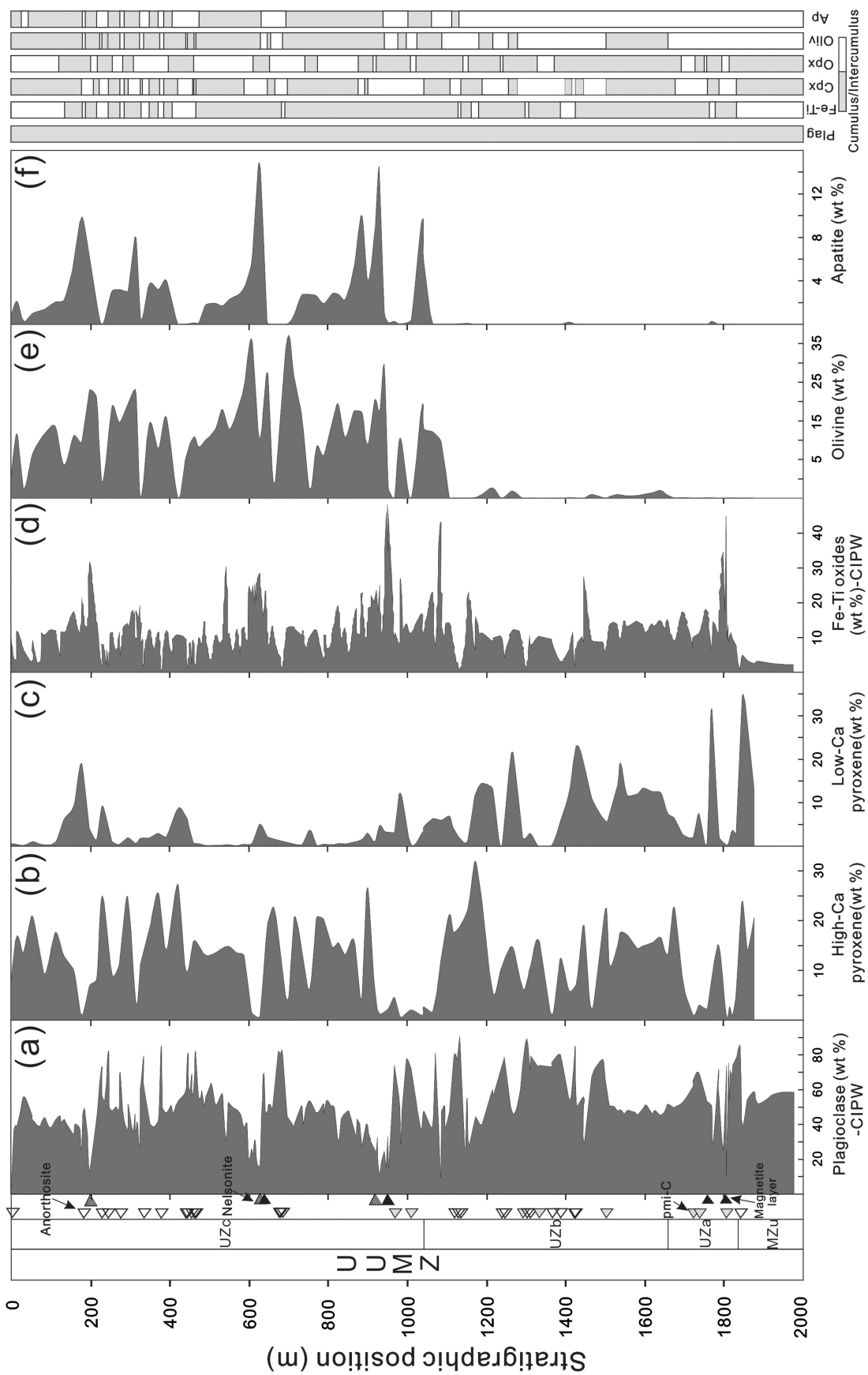

Fig. 5. Mineral modes in cumulates from the Upper Main and Upper Zone of the Bushveld complex in the Bierkraal cores for (a) plagioclase, (b) high-Ca pyroxene, (c) low-Ca pyroxene, (d) Fe–Ti oxides, (e) olivine and (f) apatite. (b), (c), (e) and (f) are based on MLA-scanning data. To the right is the stratigraphy of cumulus (grey) and intercumulus (white) phases.

Table 1: Position of anorthosite, leucogabbro and magnetite layers from the Bierkraal drill core

Sample no.	Stratigraphic position	Rock type	Subzone	Cumulate phase
BK1–666.4	229·67	Anorthosite	UZc	p
BK1–684	245·74	Anorthosite	UZc	p
BK1–718.3	276·99	Anorthosite	UZc	p
BK1–782.3	335·55	Anorthosite	UZc	p
BK1–782.45	335·61	Anorthosite	UZc	p
BK1–783.4	336·55	Anorthosite	UZc	p
BK1–830.6	379·67	Anorthosite	UZc	p
BK1–902.3	445·17	Anorthosite	UZc	p
BK1–903	445·81	Anorthosite	UZc	p
BK1–904.5	447·18	Anorthosite	UZc	p
BK1–914.99	456·76	Anorthosite	UZc	p
BK1–922.7	463·81	Anorthosite	UZc	p
BK1–923.61	464·64	Anorthosite	UZc	p
BK1–925.91	466·74	Anorthosite	UZc	p
BK1–927.5	468·19	Anorthosite	UZc	p
BK1–1155.92	676·86	Anorthosite	UZc	p
BK1–1166.52	686·55	Anorthosite	UZc	p
BK3–600	1128·23	Anorthosite	UZb	p
BK3–600.66	1128·83	Anorthosite	UZb	p
BK3–607.7	1135·26	Anorthosite	UZb	p
BK3–729.8	1246·81	Anorthosite	UZb	p
BK3–730	1246·99	Anorthosite	UZb	p
BK3–791.6	1303·26	Anorthosite	UZb	p
BK3–884.1	1387·77	Anorthosite	UZb	p
BK3–920	1420·56	Anorthosite	UZb	p
BK3–922.4	1422·76	Anorthosite	UZb	p
BK3–925	1425·13	Anorthosite	UZb	p
BK3–1380.7	1841·43	Anorthosite	UZa	p
BK1–620.5	187·73	Leucogabbro	UZc	pmi
BK1–1114.7	639·21	Leucogabbro	UZc	pmi
BK1–1160.4	680·96	Leucogabbro	UZc	pmi
BK1–1475.7	969	Leucogabbro	UZc	pmi
BK1–1476.2	969·45	Leucogabbro	UZc	pmi
BK1–1508.2	998·69	Leucogabbro	UZc	pmi
BK1–1520.4	1009·83	Leucogabbro	UZc	pmi
BK3–590	1119·09	Leucogabbro	UZb	pmi
BK3–721.3	1239·04	Leucogabbro	UZb	pmi
BK3–780	1292·67	Leucogabbro	UZb	pmi
BK3–800	1310·94	Leucogabbro	UZb	pmi
BK3–800.3	1311·21	Leucogabbro	UZb	pmi
BK3–825	1333·78	Leucogabbro	UZb	pmi
BK3–825.1	1333·87	Leucogabbro	UZb	pmi
BK3–860	1365·75	Leucogabbro	UZb	pmi
BK3–860.3	1366·02	Leucogabbro	UZb	pmi
BK3–971.5	1467·61	Leucogabbro	UZb	pmi
BK3–1000	1493·65	Leucogabbro	UZb	pmi
BK3–1010.5	1503·24	Leucogabbro	UZb	pmi
BK3–1251	1722·95	Leucogabbro	UZb	pmi
BK3–1267.8	1738·29	Leucogabbro	UZb	pmi
BK3–1342.6	1806·63	Leucogabbro	UZb	pmi
BK3–1347.5	1811·1	Leucogabbro	UZb	pmi
BK3–1348.5	1812·02	Leucogabbro	UZb	pmi
BK3–1352.5	1815·67	Leucogabbro	UZb	pmi
BK3–1356.01	1818·88	Leucogabbro	UZb	pmi
BK3–1360	1822·52	Leucogabbro	UZb	pmi
BK3–1369.9	1831·57	Leucogabbro	UZb	pmi
BK1–1119.3	643·41	Magnetite layer	UZc	pmi
BK1–1453.3	948·53	Magnetite layer	UZc	pmi
BK1–1458.12	952·94	Magnetite layer	UZc	pmi
BK1–1460	954·66	Magnetite layer	UZc	pmi
BK3–1290	1758·58	Magnetite layer	UZb	pmi
BK3–1343	1806·99	Magnetite layer	UZb	pmi
BK3–1333.95	1798·73	Magnetite layer	UZb	pmi

Stratigraphic positions are given in meters with the '0 meter' reference level (411·8 m in BK1) being a diorite. Mineral abbreviations in cumulus assemblages: p, plagioclase; m, magnetite; i, ilmenite.

within host plagioclase (Fig. 4f). Plagioclase in all these anorthositic rocks has crystallized as large laths and usually displays a good planar orientation, but many small patchy plagioclase crystals can also be observed in these samples.

The main cumulus minerals of UUMZ are plagioclase, high-Ca pyroxene, olivine, low-Ca pyroxene, magnetite, ilmenite and apatite. Biotite, hornblende, sulphide, quartz and K-feldspar are common accessory minerals; cumulus K-feldspar, quartz and amphibole also appear in the ferrodiorite at the top. It is noteworthy that the main cumulus minerals in UZa and UZb are significantly coarser than those in UZc, especially for plagioclase, pyroxene and olivine. Fe–Ti oxides are mainly composed of magnetite with minor ilmenite. However, ilmenite dominates the Fe–Ti oxide minerals in the ferrodiorite at the top of UUMZ.

Mineral occurrence and modes

MZu is the lowest part of the UUMZ and has been well studied by Cawthorn *et al.* (1991). Our samples include only a small interval of MZu, which is mostly gabbronorites. Plagioclase occurs as strongly tabular euhedral to subhedral grains and pyroxenes generally are subhedral grains 2–4 mm in size (Fig. 3a). In MZu (from 1877 to 1845 m), the modal proportions of plagioclase decrease gradually from 63 to 38 wt % whereas the low-Ca pyroxene modal proportions increase progressively from 13 to 34 wt % from the bottom up, with high-Ca pyroxene ranging between 14 and 24 wt % (Fig. 5).

After magnetite saturation in UZa, the samples are dominated by pmi-C with a few magnetite gabbronorites. Plagioclase in UZa forms large grains defining a magmatic lamination and smaller, randomly oriented grains are commonly located around the large cumulus phases or within Fe–Ti oxide patches (Fig. 3b and c), which suggests recrystallization of the original plagioclase. High-Ca pyroxene crystals usually form large sub-equant grains with irregular boundaries and are frequently twinned (Fig. 3b). Inverted pigeonite contains coarse exsolution lamellae of augite or irregular and sub-orbicular augite. In UZa, the samples show large variations in the modal proportions of plagioclase (10–78 wt %), high-Ca pyroxene (1–23 wt %), and low-Ca pyroxene (0–32 wt %). Fe–Ti oxides range from 11 to near 80 wt % in the MML from 1831 to 1807 m (Fig. 5d).

In UZb, the rocks are mainly composed of plagioclase, high-Ca pyroxene and low-Ca pyroxene, with some olivine and Fe–Ti oxides. Plagioclase in UZb is similar to that in UZa, with the grain size ranging from 0·1 to 4 mm. High-Ca pyroxene is a ubiquitous phase crystallized as equant to slightly prismatic euhedral grains with a size range from 0·2 to 2 mm (Fig. 3c). Low-Ca pyroxene is dominated by inverted pigeonite, but hypersthene is also present, with the latter mainly occurring as sub-equant to euhedral prismatic grains in the gabbronorite (Fig. 3c). Inverted pigeonite is subhedral with exsolution lamellae of augite or occurs as oikocrystic patches. Olivine usually forms sub-equant large grains, locally with a prismatic shape (Fig. 3c).

In UZb, from 1659 to 1428 m (Fig. 5), the mineral proportions are relatively constant with plagioclase (46–52 wt %), high-Ca pyroxene (7–19 wt %), low-Ca pyroxene

(8–20 wt %), about 1–2 wt % olivine and a broadly decreasing trend in Fe–Ti oxides from 15 to 7 wt % (with the exception of few pmi-C samples in the upper part). The interval from 1428 to 1293 m is dominated by a series of anorthositic samples (or pmi-C) with plagioclase proportions varying between 71 and 88 wt % and a progressive decrease in low-Ca pyroxene from 13 to 2 wt % (Fig. 5). Modal proportions for Fe–Ti oxides vary from 2 to 12 wt %, and for high-Ca pyroxene from 1 to 16 wt %. In the upper part of UZb from 1283 to 1064 m, although there are still some anorthosites and pmi-C samples, plagioclase first increases to 78 wt % in the first 37 m and then gradually decreases to around 27 wt % from depth 1247 to 1147 m. After that, the plagioclase mode again sharply increases to 89 wt % at 1135 m and then roughly decreases to 2 wt % in a magnetite layer at 1084 m. Other mineral phases in this interval change significantly, with Fe–Ti oxides ranging from 1 to 43 wt %, high-Ca pyroxene from 2 to 32 wt % and low-Ca pyroxene from 0 to 22 wt % (Fig. 5).

In UZc, the assemblages are mainly magnetite–olivine gabbro and magnetite-troctolite (Fig. 5). Plagioclase is tabular, subhedral to euhedral, with a relatively small size (0·2–3 mm) (Fig. 3d and e) and usually exhibits a planar orientation (Fig. 3e). High-Ca pyroxene crystallized as smaller sub-equant to subhedral grains oriented along the magmatic lamination and typically with abundant Fe–Ti oxide exsolution (Fig. 3e). In UZc, olivine forms small (0·3–2 mm) equant to irregular tabular grains (Fig. 3d and e). Apatite is a cumulus phase and typically forms small sub-rounded grains (*c.* 0·2 mm), commonly embedded in Fe–Ti oxides (Fig. 3d). In UZc, apatite appears rhythmically after its first appearance as a cumulus phase at a depth of 1042 m. In each cycle, apatite is almost absent before saturation then reaches very high modal proportions before declining smoothly upwards (Fig. 5f). This pattern repeats several times in UZc.

GEOCHEMICAL DATA

Major elements in whole-rocks

Major and trace element compositions of whole-rock samples are presented in Supplementary Data Table S1. Our data for P_2O_5 concentrations compare very well with the data of Cawthorn & Walsh (1988) in the same drill cores. It is therefore appropriate to combine their data with our new dataset.

Generally, Bierkraal samples show large compositional variations for most major elements (Fig. 6); FeO_{tot} varies from 2 to 63 wt %, showing a negative linear relationship with SiO_2 (10–57 wt %); CaO ranges from 6 to 12 wt %, except for the very low CaO content present in magnetite-rich rocks; Al_2O_3 ranges from 6 to 27 wt % and positively correlates with the variation of SiO_2; P_2O_5 ranges from 0 to 6 wt %. The variation of Na_2O and K_2O is broadly correlated with SiO_2 and changes from 0 to 5 wt % and from 0 to 1·3 wt % respectively. In addition, TiO_2 varies from 0 to 16 wt % and displays a clear negative relationship with SiO_2. MgO is relatively low (<7 wt %) in most samples, with whole-rock Mg# [100MgO/(MgO + FeO_{tot})] values less than 40.

Stratigraphically, $FeO_{tot} + TiO_2$ first gradually increases to 70–76 wt % from the bottom of the UUMZ to the MML, and then decreases erratically upward from 76 to 12 wt % at about 1500 m. From 1500 to 1043 m, this parameter broadly displays five cycles, each with a progressive increase from <10 wt % to more than 40 wt %, followed by a rapid decline to very low values (<10 wt %) (Fig. 7a).

In the uppermost portion (above 1043 m) in UZc, most major elements display a cyclic behavior as represented by the bulk-rock P_2O_5 content. At the bottom of each cycle P_2O_5 is low (<0·3 wt %), then increases to 3–5 wt % within 15 m, and rapidly decreases to *c.* 0·9 wt % over about 100 m, and finally drops rapidly (over <1 m) to much lower values (0–0·2 wt %), as apatite becomes a minor interstitial phase (Fig. 7b). This pattern, which is repeated four times for both P_2O_5 and other major elements (FeO_{tot}, TiO_2) (Fig. 7a), is strongly correlated with the modal variations of apatite and Fe–Ti oxides.

Mineral composition

Correlation between mineral compositions

The compositional variations of minerals exhibit a broad fractionation trend across the UUMZ stratigraphy for plagioclase ($An_{71–35}$) (Supplementary Data Table S2), high-Ca pyroxene ($Mg\#_{74–5}$) (Supplementary Data Table S3), olivine ($Fo_{55–1}$) (Supplementary Data Table S4), and low-Ca pyroxene ($Mg\#_{72–23}$) (Supplementary Data Table S5) (Fig. 8). The plagioclase composition evolves concomitantly with the high-Ca pyroxene and low-Ca pyroxene composition from An_{71} and $Mg\#_{72}$ to the points around at An_{53} and $Mg\#_{44–55}$. The evolution trend becomes steeper slightly before apatite appearance (Fig. 8a and b). Olivine is characterized by an evolution from Fo_{45} at An_{56} to Fo_{14} at $An_{47–52}$ followed by a change to $Fo_{1–5}$ at An_{40} with a less steep slope in the top 80 m (Fig. 8c). Additionally, Fo in olivine is linearly correlated with Mg# in high-Ca pyroxene from Fo_{50} to Fo_{10}, with a change to a steeper slope after Fo_{10} in the top ferrodiorite rocks (Fig. 8d).

Stratigraphic evolution of mineral compositions

The MZu (from depth 2070 to 1845 m) is represented by a smooth fractionation trend in the composition of plagioclase (An 63–58; Fig. 9a), high-Ca pyroxene (Mg# 72–65; Fig. 9b) and low-Ca pyroxene (Mg# 63–59; Fig. 9d). However, the up-section decrease of the plagioclase anorthite component is interrupted between 1841 and 1823 m depth, where it gradually increases from 57·8 to 61·5. Nine additional reversals in plagioclase composition (between 2 and 5% An) occur in UZa and UZb between 1831 and 1043 m depth, at an

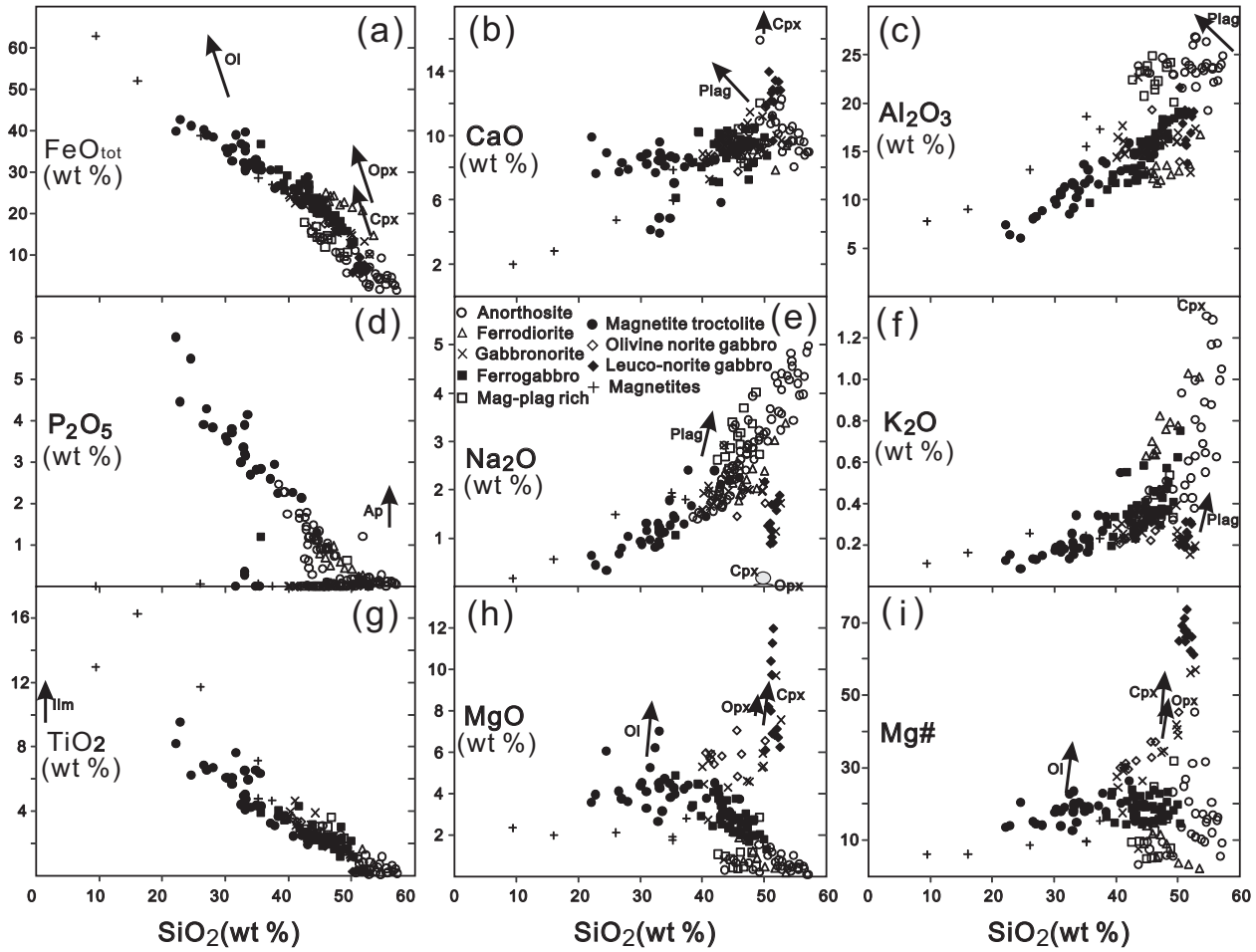

Fig. 6. Major element variation diagrams for bulk-rocks from the UUMZ of the Bushveld Complex. Data are from Supplementary Data Table S1. The arrows in each panel indicate the differentiation effects of various minerals from the bottom to the most evolved section.

interval of 30–90 m. In UZc, seven significant reversals in plagioclase composition (between 5 and 10% An) are also observed at a relatively larger spacing. All these 17 reversals in plagioclase composition are larger than the analytical error and the compositional variation within a single sample (2% An; Supplementary Data Table S2).

For high-Ca and low-Ca pyroxenes, Mg# variations (of about 110 samples) also record an overall up-section variation in the evolution trend. However, many significant reversals of Mg# (Mg# 4–24%) in high-Ca and low-Ca pyroxenes are observed and are concomitant with the reversals recorded by anorthite content in plagioclase. The most remarkable reversals in Mg# of the high-Ca pyroxene occur at stratigraphic depths of 686–648 m (25–48·5), 446–442 m (28·6–47) and 246–200 m (31–51). From the bottom, the Mg# of high-Ca pyroxene decreases smoothly from 72 to 65 before it exhibits a small reversal from 65 to 67, which is also accompanied by a reversal in plagioclase composition (An 58–61). Similar reversals documented by both high-Ca pyroxene and anorthosite occur several times in UZb. However, we also note two reversals, from 1531 to 1503 m and from 1216 to 1172 m, where the Mg# of the low-Ca pyroxene is opposite to the reversals observed in plagioclase composition (Fig. 9a and d). In the whole stratigraphic sequence and in particular in UZc the Mg# in both pyroxenes shows similar evolution and similar reversals (Fig. 9b and d).

Cr and V in bulk-rocks and in magnetite

The evolution of Cr in bulk-rock, as a function of stratigraphic position, is presented in Fig. 10a. Cr content reaches the highest value at a depth of 1846 m, slightly before magnetite saturates, then it decreases progressively to the detection limit near 1800 m depth. This pattern occurs again from 1758 to 1500 m. From 1500 to 1000 m depth, the value of Cr fluctuates between low ($<$12 ppm; detection limit is *c.* 5 ppm) and high values ($>$40 ppm) on a scale of $\sim$50 m. In the upper 1000 m of the section Cr is around 5–8 ppm, except for a few samples that have much higher values (Fig. 10a). V in bulk-rocks is shown in Fig. 10b. At a first glance V values can

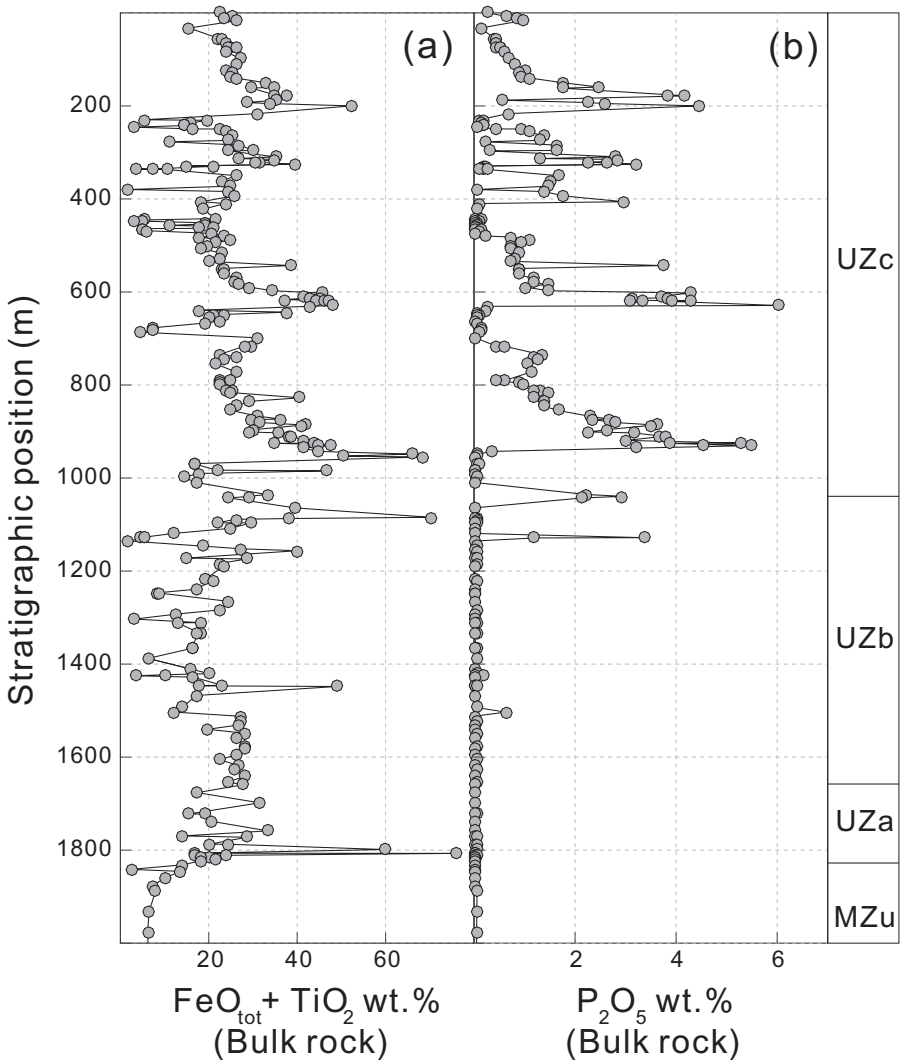

Fig. 7. Stratigraphic evolution of bulk-rock compositions for (a) $FeO_{tot} + TiO_2$ (wt %) and (b) P_2O_5 (wt %). Data are listed in Supplementary Data Table S1.

be separated into two parts. The lower part of the section exhibits a gradual increase to 1800 ppm in the first 120 m (1877–1758 m). Bulk-rock V concentrations then broadly decrease to 200 ppm near 1000 m depth. Most samples in the upper part have significantly lower values (<100 ppm).

Published values of Cr in magnetite separates from 237 samples are shown in Fig. 10c (Supplementary Data Table S7; data from Maila, 2015). Overall, the variation pattern of Cr in magnetite with stratigraphy correlates very well with the bulk-rock contents of our samples (Fig. 10a and c). The Cr content in magnetite clearly shows a number of reversals and some of the peak values are documented by a continuous series of samples (Fig. 10c). In particular, most of the reversals in Cr are broadly correlated to the anorthositic intervals; Cr and anorthite content of plagioclase reversals correlate well.

DISCUSSION

Comparison between Bushveld limbs

The three major limbs (western, eastern and northern) of the Bushveld Complex are very similar in terms of the uppermost layers that form the UUMZ (von Gruenewaldt, 1973; Molyneux, 1974; Ashwal *et al.*, 2005). The western and eastern limbs display striking similarity and have been confirmed to be connected through the center at depth based on geophysical data (Webb *et al.*, 2011). The broadly similar thickness of several famous layers (PM, MML and Magnetite Layer 21) in the UUMZ further demonstrates their relationship. In addition, the cyclicity in bulk-rock P_2O_5 after apatite saturation, described in this study, correlates extremely well with the data from UZc at Roossenekal for the eastern limb (Scoon & Mitchell, 2012) (Fig. 11a). The section from 1400 to 1600 m at Roossenekal is speculated to

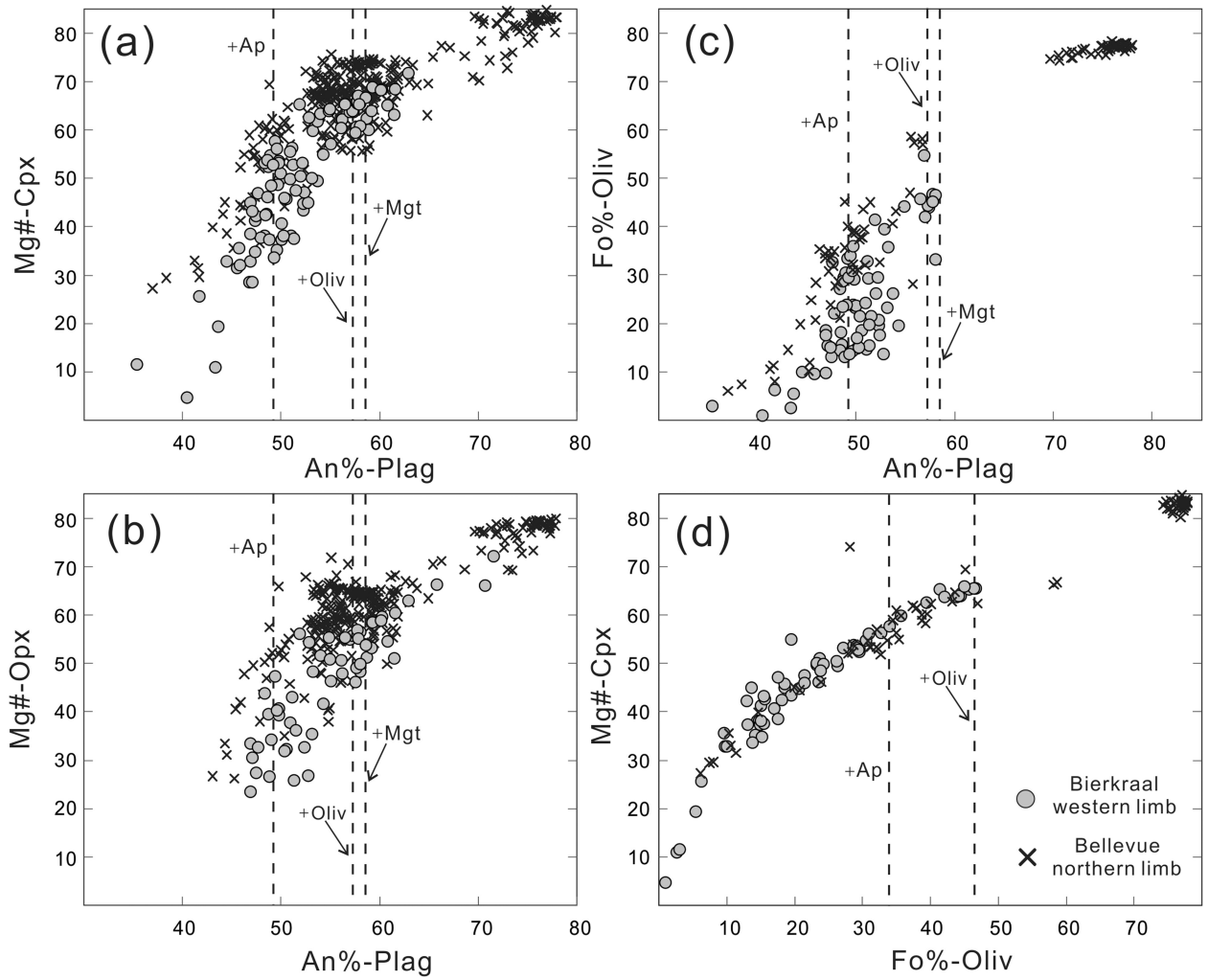

Fig. 8. Compositions of coexisting mafic silicates and plagioclase from the Bierkraal and Bellevue drill cores. (a) An % in plagioclase vs Mg# in high-Ca pyroxene; (b) An % in plagioclase vs Mg# in low-Ca pyroxene; (c) An % in plagioclase vs Fo % in olivine; (d) Fo % in olivine vs Mg# in high-Ca pyroxene. Plag, plagioclase; Oliv, olivine; Ap, apatite; Mgt, magnetite. The data for Bellevue are from the study of Ashwal *et al.* (2005) (Supplementary Data Table S9).

have been affected by abundant dolerite dykes. However, we notice that the pattern of phosphorus variation in the same stratigraphic location nearby in the eastern limb (Supplementary Data Table S8; VanTongeren *et al.*, 2010) is consistent with the western limb at Bierkraal (Fig. 11b). This confirms the lateral consistency of lithological variation between eastern and western limbs.

The relationship between the UUMZ of the northern limb and the rest of the Complex is controversial (Ashwal *et al.*, 2005). The mineral compositions from the Bellevue core published by Ashwal *et al.* (2005) (Supplementary Data Table S9) are shown in Fig. 8, together with the data collected in this study. Mineral variations in the Bellevue core are generally similar to those observed in Bierkraal. Exceptions are the primitive troctolitic rocks at the bottom of the Bellevue core ($An_{>65}$) (Fig. 8a–c), which are not observed in Bierkraal, and the extremely evolved rocks in Bierkraal ($Fo_{<10}$) (Fig. 8d), which are not seen in Bellevue. Another significant difference between the Bierkraal and Bellevue sections is the obvious different thickness of UZa and UZc (Fig. 2) and the presence of thick granite and dolerite sills (Ashwal *et al.*, 2005) in UZc in Bellevue.

Our detailed stratigraphic and geochemical comparisons confirm that the eastern and western limbs are extremely similar in the UZc and are likely to be connected at depth. In contrast, the Bellevue section in the northern limb shows differences in mineral compositions and lithology, so that the connectivity with the other limbs remains uncertain.

Compositional reversals in Bierkraal drill cores

Progressive mineral reversals have been widely documented in the Bushveld (Pyroxenite Marker of the Bushveld, Cawthorn *et al.*, 1991; VanTongeren & Mathez, 2013) and in other well-studied layered intrusions (Fongen–Hyllingen, Wilson & Sorensen, 1996;

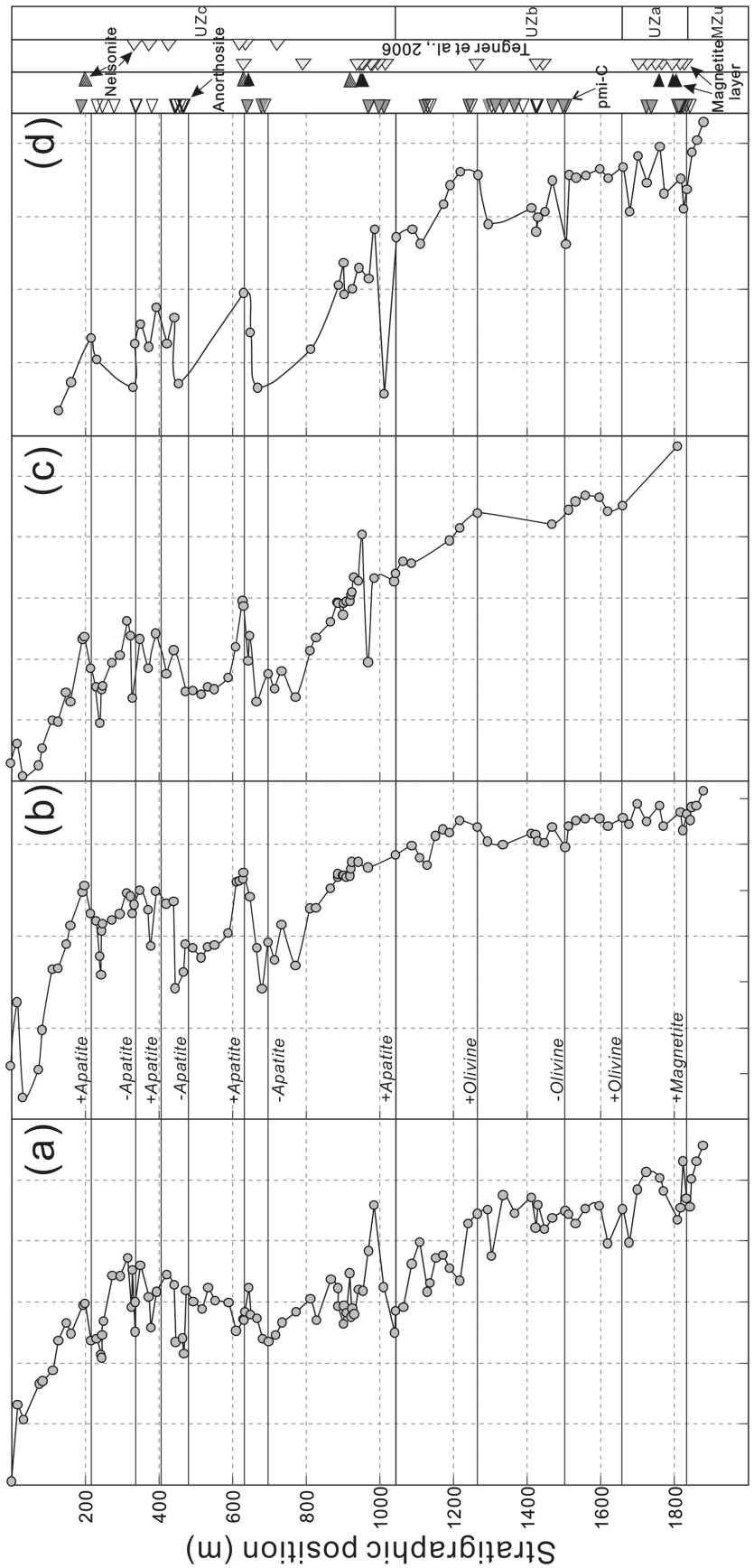

Fig. 9. Compositional variation of (a) plagioclase (An %), (b) high-Ca pyroxene (Mg#), (c) olivine (Fo %) and (d) low-Ca pyroxene (Mg#), with stratigraphic position in the Bierkraal drill cores. Data are from Supplementary Data Table S2–S5.

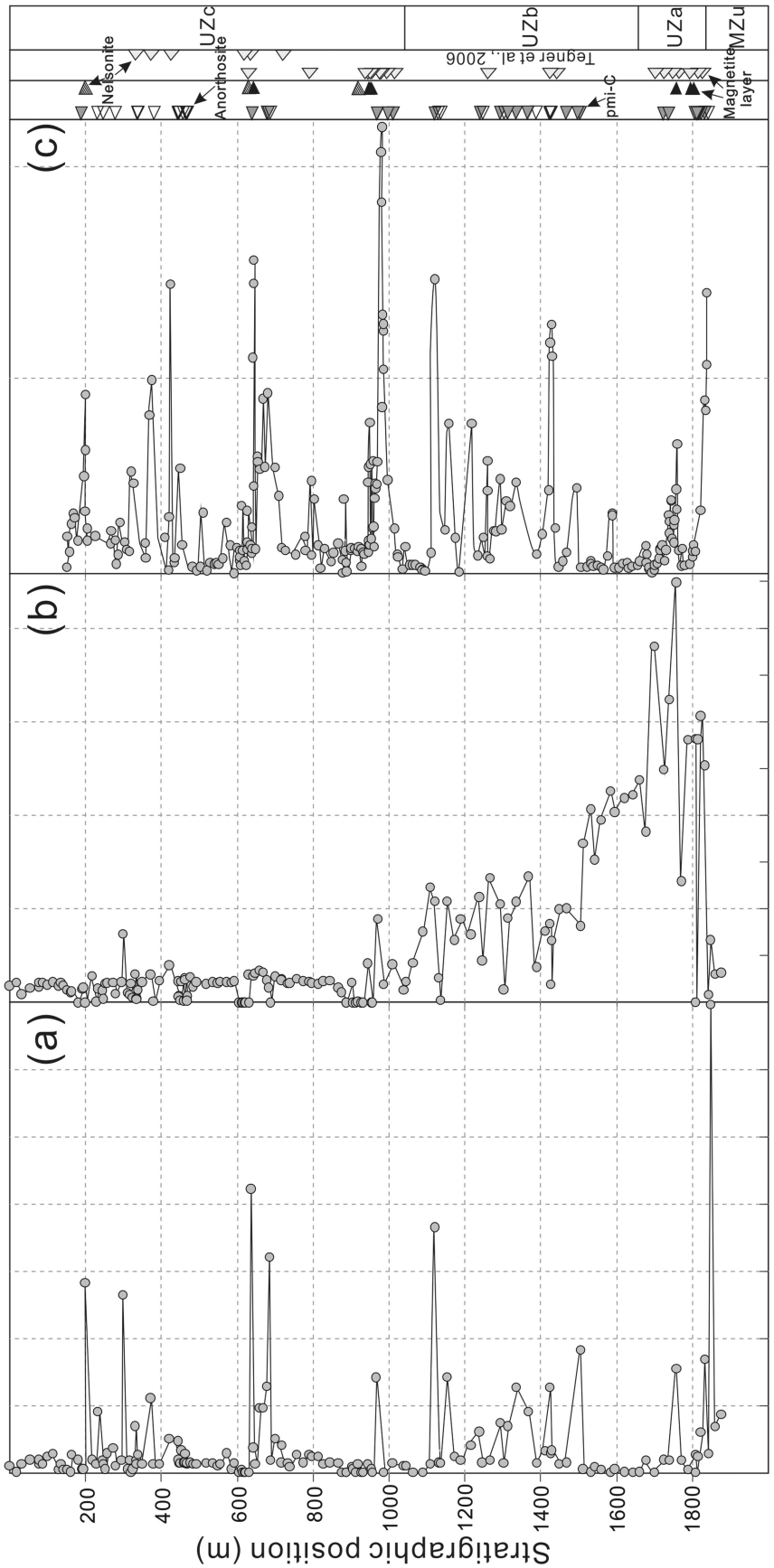

Fig. 10. (a) Concentration of Cr in bulk-rocks; (b) V in bulk-rocks; (c) Cr in magnetite separates vs stratigraphic position in the Bierkraal drill cores. Data for Cr in magnetite separates are from Maila (2015).

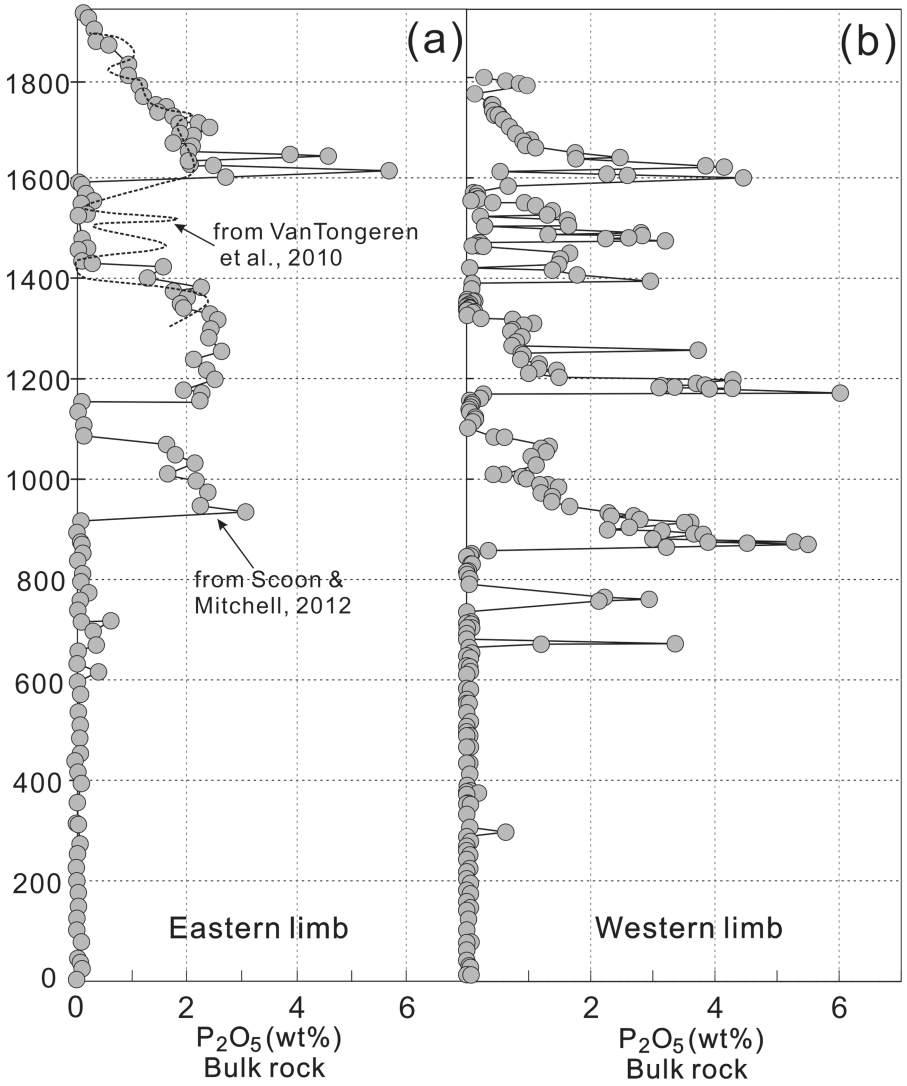

Fig. 11. Compositional variation of bulk-rock P_2O_5 (wt %) in the Upper Zone from the eastern (a) and western (b) limbs of the Bushveld. The '0 meter' reference level is based on the MML in both limbs. (a) is modified after Scoon & Mitchell (2012). Samples from VanTongeren *et al.* (2010) were collected from Magnet Heights and the Droogehoek area, whereas the samples reported by Scoon & Mitchell (2012) are from the Roossenekal district.

Sept Iles, Namur *et al.*, 2010). Such reversals are typically regarded as indicators of new magma recharge and mixing with the resident melt in the magma chamber. Reversals in mineral compositions in the Bushveld UUMZ have also been previously reported in the northern limb (Ashwal *et al.*, 2005) and the western limb (Tegner *et al.*, 2006).

For the Bierkraal data presented here, reversals have been identified in whole-rock and mineral compositions and are used to define cycles. Trapped liquid shift effects may change the composition of mafic minerals (Barnes, 1986), but have no influence on plagioclase core compositions (Grove *et al.*, 1984). We therefore define the boundaries between cycles as the lowest anorthite content within each reversal. Gradual increases in anorthite content, the Cr content in magnetite separates, and the Mg# of high-Ca pyroxene are usually observed above the level of these minimum values. Following the reversal, these parameters usually exhibit a continuous decrease before the next cycle starts. Importantly, we observe that most of the reversals are closely associated with anorthosite or pmi-C rocks, which are usually located at the bottom of the cycles (cycle II, III, VIII, IX, XI, XIII–XVI and XVIII) (Fig. 12).

Some of the reversals that we documented are stratigraphically close to reversals previously described by Tegner *et al.* (2006), such as those cycles defined by the disappearance of apatite (Fig. 12c). In Fig. 12 four mineral or bulk-rock compositional indices (Cr in magnetite, An %, P_2O_5 and Mg# in high-Ca pyroxene) are compared to illustrate these compositional variations. The reversals in UZa and UZb are best represented by Cr in magnetite and An in plagioclase, whereas the reversals in UZc are documented perfectly by all four indices (Fig. 12).

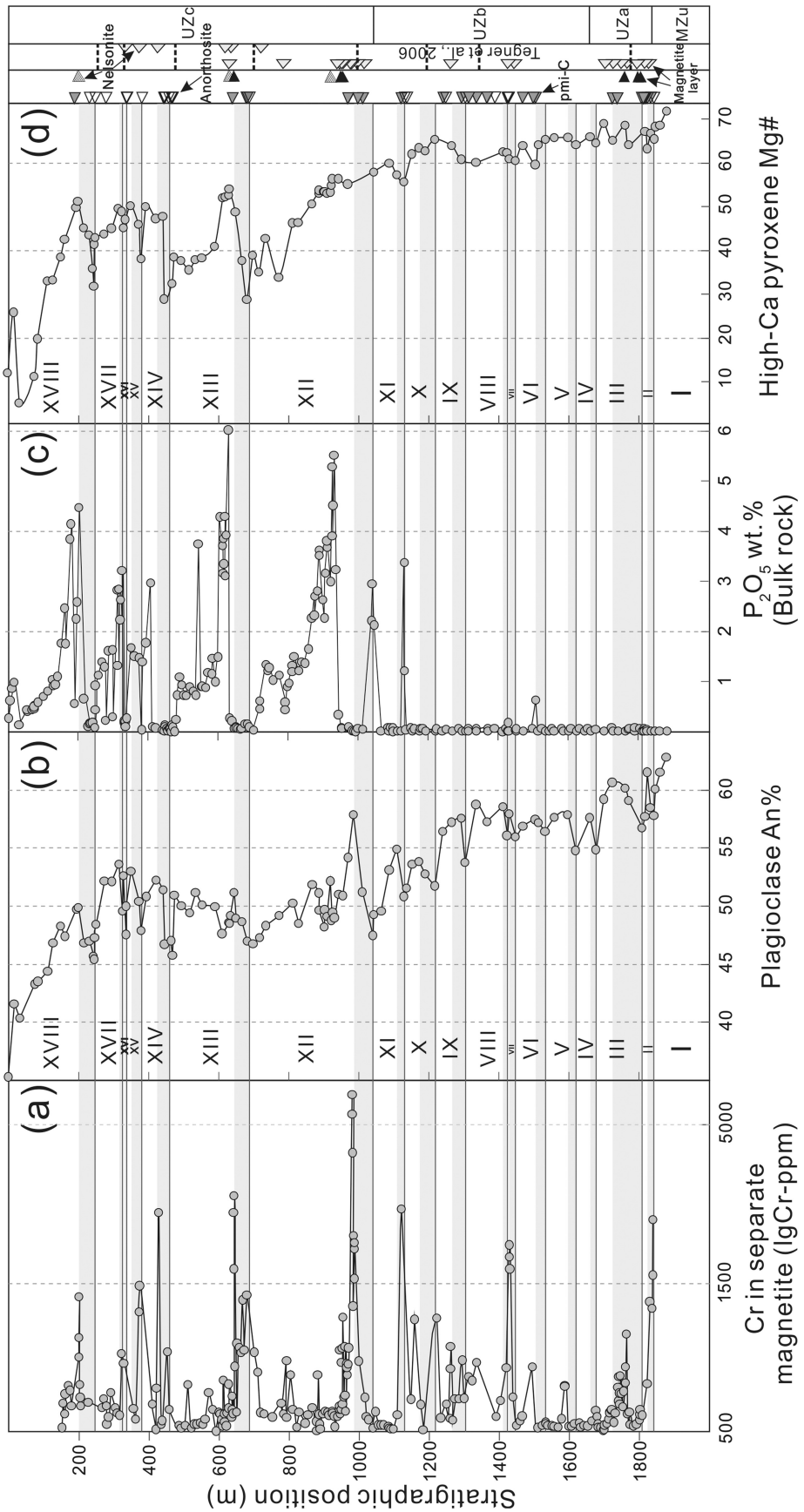

Fig. 12. (a) Compositional variations of Cr in magnetite separates; (b) plagioclase An %; (c) bulk-rock P_2O_5 variation; (d) Mg# in high-Ca pyroxene, with stratigraphic position in UUMZ. Data for Cr in magnetite separates are from Maila (2015). Fine horizontal lines represent the boundaries between cyclic units.

Lithological cycles

UZa and UZb display cyclic patterns in FeO_{tot} above 1500 m, which correspond to a typical lithological sequence from anorthosite to leucogabbro, then to magnetite (olivine) gabbro/norite to oxide-rich layers, and then sharply to pmi-C rocks or anorthosite (Fig. 13a and b). Locally the base of the sequence starts with leucogabbro (1503–1441 m) or ends with no magnetite layer (1247–1156 m). Magnetite layers in the Bierkraal drill cores (Tegner *et al.*, 2006) usually occur above the magnetite (olivine) gabbro/norite (Supplementary Data Fig. S3).

UZc rocks consist of magnetite gabbro and magnetite troctolite with magnetite, nelsonite and anorthosite layers (Figs 3 and 4). The most conspicuous feature in UZc is the cyclicity of modal apatite (Figs 5f and 7b). Commonly the bottom of each cycle starts with leucogabbro and/or anorthosite. The plagioclase proportion gradually decreases to about 20 wt % in the magnetite-rich samples and apatite appears as a major cumulus phase in the upper portions of these magnetite-rich rocks, forming nelsonite layers. Higher up, the apatite proportion progressively decreases to 0·8–1 wt % and then declines sharply to near zero with the assemblage changing from magnetite troctolite to ferrogabbro and leucogabbro (Fig. 13c and d). Concomitantly, the modal proportion of plagioclase behaves in an opposite way to the trend of apatite, starting with about 20 wt % plagioclase in magnetite troctolite, then gradually increasing to about 50 wt % in ferrogabbro, and jumping to 80 wt % in plagioclase-rich rocks (Fig. 13c). This pattern of apatite and plagioclase proportions occurs at intervals of 1040–687 m, 687–468 m and 246–0 m, except in the interval of 468–246 m where the samples show an alternation of anorthosite and ferrogabbro (with apatite) on a small scale of about 40 m. In UZc, the evolution trend in Fe–Ti oxides is very similar to that in P_2O_5, but it is observed that not all magnetite layers contain cumulus apatite and usually the nelsonite is found slightly above the magnetite layers (Fig. 13d), which indicates different settings for them.

Continuous fractionation *vs* magma replenishment

A recent model incorporating repeated slumping and collapse of a crystal-mush has been proposed for the formation of layering in the Bushveld Complex (Maier *et al.*, 2012), but it is unclear whether a single unifying hydrodynamic process is able to explain the full nature of the layering observed in the entire Bushveld Complex (Scoon & Mitchell, 2014). In a detailed study of the UZ at Bierkraal, Tegner *et al.* (2006) identified nine cycles within the UUMZ, interpreted as resulting from magma mixing between two magma layers within a stratified magma chamber. According to the model presented by Tegner *et al.* (2006), magnetite crystallization leads to a decrease in the melt density of the basal layer, and, when the melt density becomes equal to that of the overlying layer, the diffusive boundary between the magma from the two layers breaks down and mixing occurs.

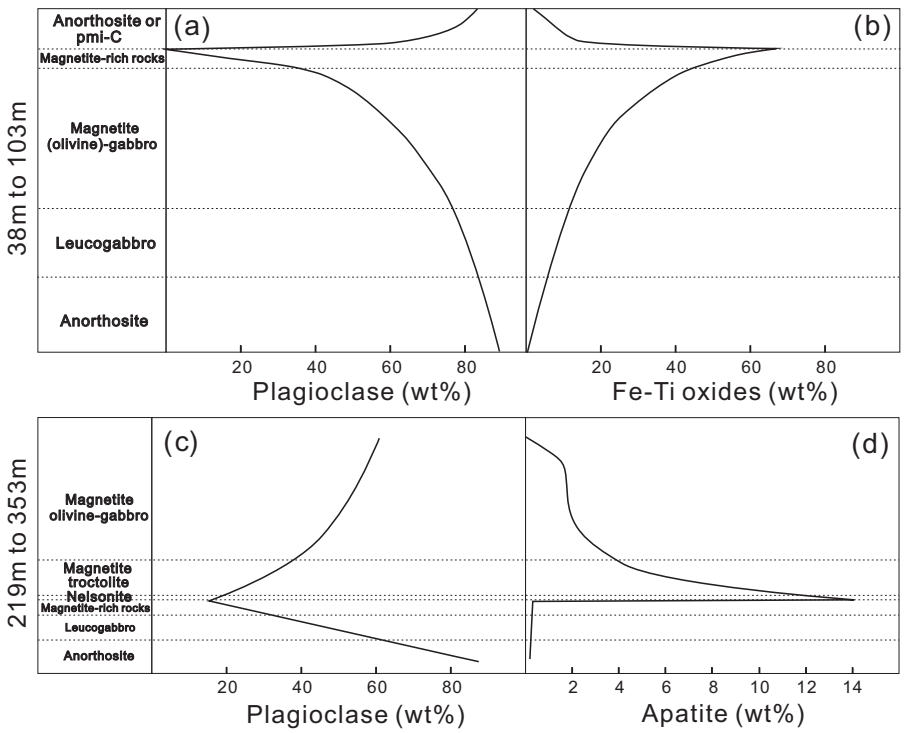

Fig. 13. Schematic lithological section through an idealized cyclic sequence in UZb (a, b) and UZc (c, d). (a) and (b) are based on the interval from 1841 to 1749 m in UZb. (c) and (d) are based on the ideal unit between 690 and 470 m. In some units, some horizons may be missing.

However, our sampling at <10 m intervals shows that only the first reversal has a close relationship with the appearance of Fe–Ti oxides. The other 16 reversals do not have new cumulus phases or a magnetite layer that can significantly change the melt density. The reversals in cycles III, VII, VIII and X are even characterized by the disappearance of magnetite (1769 m, 1428 m, 1410 m and 1172 m depth, respectively). Consequently, we argue that the UUMZ cumulates were not formed by closed-system differentiation but, in contrast, crystallized from a series of magma pulses.

At the bottom of the UUMZ, from the PM to the first appearance of cumulus Fe–Ti oxides, the samples display a near-continuous trend of upward decreasing anorthite content in plagioclase, $Mg\#_{cpx}$ and $Mg\#_{opx}$. This trend lasts from 1877 to 1841 m, followed upwards by 17 reversals at a scale of 30–340 m (Fig. 12). Although some of these reversals are characterized by a minor increase of anorthite in plagioclase (2–3 An %), the majority are related to substantial increases in An %, Fo content and $Mg\#_{cpx}$, documented in several successive samples such as the reversal in cycles III (An 56·8–61), XI (An 51–55), XIII (An 47–51), XIV (An 45·8–52·3), XV and XVI (An 48–53), XVIII (An 45–50), and the marked increase in An of about 22 mol % from 1039 to 985 m depth in cycle XII (An from 47·5 to 58). The two most obvious reversals in cycles XII and XIII are highlighted to show the concurrent reversals in An in plagioclase and Cr in magnetite separates, and particularly to illustrate the relationship of magnetitite and nelsonite (Fig. 14). The significant reversal in An in cycle XII has also been confirmed by a detailed study of An in separated plagioclases from the same drill core (Lum, 2011). These large variations clearly suggest perturbation in the crystallization process and strongly argue against closed-system crystal fractionation for the UUMZ. In addition, within several reversal intervals (cycles XII to XV and XVIII), there is also a remarkable increase of V_2O_5 content in magnetite (Cawthorn & Walsh, 1988). Similarly, in the detailed study of the UUMZ of the Bellevue drill core (northern limb), Ashwal *et al.* (2005) attributed the reversals of An in plagioclase and Mg# in pyroxene to new magma replenishments. Importantly, as discussed above, the almost simultaneous reversals of Cr in magnetite (Fig. 12a) and anorthosite in plagioclase (Fig. 12b) present unarguable evidence for primitive magma recharge for the UUMZ.

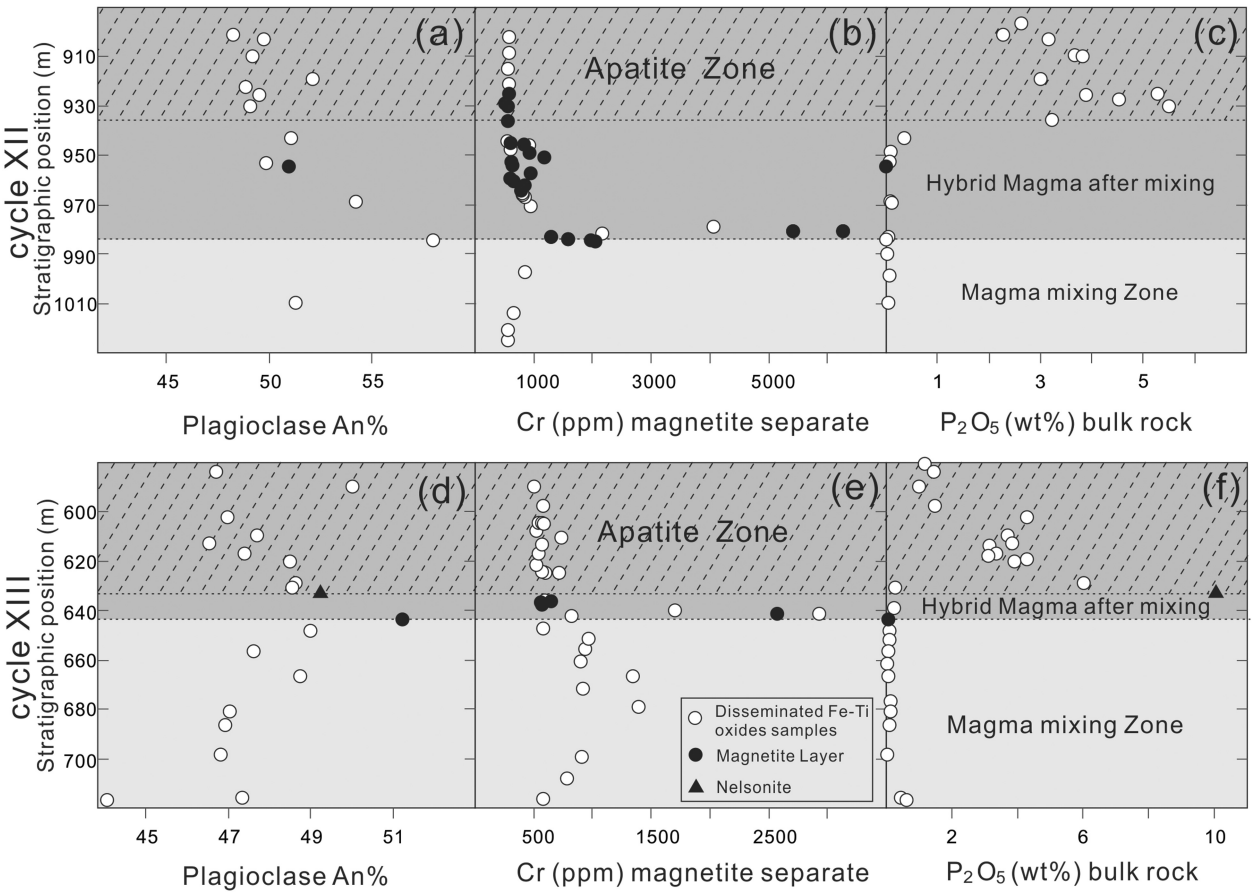

Fig. 14. Details of cycles XII and XIII showing the concomitant reversals in An content of plagioclase (a, d) and Cr in magnetite separates (b, e), and illustrating the phosphorus-rich zones in each cycle (c, f). The data for Cr in magnetite separates are from Maila (2015); other data are from this study. Some magnetite layer samples in the upper part of (b) and (e) should be the nelsonites, which were not mentioned in the Maila (2015) study.

Plagioclase mush emplacement and anorthosite formation

As mentioned in the petrography section, pmi-C rocks are common in UZb (Fig. 4). This assemblage almost disappears in UZc and is replaced by a series of anorthosite layers. These layers are found in the intervals where cumulus apatite disappears in the upper cycles (Fig. 5). The most remarkable feature of these plagioclase-rich horizons in the entire UZ is that most of them are within or near the reversals documented in anorthite content in plagioclase. Some of these plagioclase-rich rocks occur at the top of the reversals and some are located within the reversals, whereas the majority of such rocks lie at the bottom of these reversals. Where such rocks are located at the base of the cycle, a gradual decrease in plagioclase proportion is observed, with a progressive petrographic trend from anorthosite to leucogabbro to gabbroic rocks. This phenomenon is best displayed in cycles XI and XII, where reversal bases are plagioclase-rich (~80 wt %) and then gradually change to a magnetite troctolite with about 20 wt % plagioclase (Fig. 13c) and a sharp increase in apatite. In UZa and UZb, an idealized cyclic unit comprises layers of anorthosite and pmi-C rocks, then magnetite (olivine) gabbro/norite and oxide-rich samples as described above. Moreover, most of these pmi-C samples in the entire UUMZ have high Cr contents in magnetite (Maila, 2015).

Overall, all these features strongly suggest that the replenishing magma carried plagioclase crystals. According to the thickness ratio between the plagioclase-rich interval (52 m) and the total cycle thickness of cycle XII (296 m), which exhibits the most typical pattern, the plagioclase load of the replenishing magma is estimated at about 15–20 vol. %. This amount of plagioclase phenocrysts is similar to that proposed in recent studies suggesting that most injected magmas can carry crystals at concentration of up to 55 wt % (Marsh, 2013).

However, whether these plagioclase crystals are formed in the feeder zone or on the way to the Bushveld magma chamber is not clear. Recent work on plagioclase crystallization during H_2O- and H_2O–CO_2-saturated magma decompression indicates that deep H_2O–CO_2 fluids could leave a lasting textural 'fingerprint' on erupted magmas (Riker *et al.*, 2015), which may correlate with the alteration in some plagioclase-rich samples. In addition, emplacement of a plagioclase-rich mush has been proposed to explain the thick anorthosite layers in other layered intrusions (Raedeke, 1982; Czamanske & Bohlen, 1990; Bédard *et al.*, 2007). Based on the magnetic susceptibility and non-cotectic proportions of plagioclase, it has been suggested that this process may have occurred in the UUMZ and in the Lower Main Zone, implying the existence of a sub-Bushveld magmatic staging chamber (Ashwal *et al.*, 2005; Roelofse & Ashwal, 2012; Roelofse *et al.*, 2015; Hayes *et al.*, 2017). Importantly, as observed in our data, the most primitive plagioclase crystals within the reversal of each cycle nicely follow the overall differentiation trend of the UUMZ (Supplementary Data Fig. S4), which also indicates that the staging subchamber is continuously differentiating. Therefore, we conclude that the reversals documented in our study of the Bierkraal drill core samples are caused by the emplacement of plagioclase-laden magmas, leading to the formation of plagioclase-rich layers within the reversal intervals of the UUMZ.

Origin of pmi-C rocks and magnetite layers in UZa and UZb

Substantial pmi-C horizons (including magnetite layers) are characteristic mineral assemblages within most cycles in UZa and UZb, but are mostly absent in UZc. Although the model of plagioclase mush emplacement can explain the basal anorthosites, another process is needed to account for the pmi-C and oxide-rich rocks in UZa and UZb.

Several lines of evidence indicate that the pmi-C assemblage is produced by a hybrid melt created by magma mixing between the resident magma and the liquid of the new plagioclase-bearing batch. First, the UUMZ sequences exhibit clear evidence for mush emplacement as documented above. The emplacement of plagioclase-laden magma and the formation of anorthosite were then followed by mixing between the resident magma and the new magma batch. Magma mixing produces a hybrid melt that can be saturated in uncommon mineral assemblages (such as plagioclase and Fe–Ti oxides in this study). This is also confirmed by the first occurrence of magnetite (1832 m), which is in a pmi-C rock (Fig. 4f). The high Cr and primitive anorthite content of these pmi-C rocks also indicate a correlation with the replenishing magma. A similar hybrid liquid with a magnetite/feldspar ratio of 30/70 has been observed in an experimental study by Roeder & Osborn (1966). Differences in the magnetite:plagioclase ratios in our samples can be explained by post-depositional modification. The PM, about 300 m below our cycle I, contains no Fe–Ti oxides. We therefore argue that some degree of fractionation, leading to the enrichment of FeO before magma mixing, is also needed to produce these pmi-C rocks.

Magnetite layers in the Bierkraal drill cores have been extensively studied and reported in previous publications. These layers commonly show a sharp lower contact with underlying anorthosite and a gradual contact with overlying anorthosite (McCarthy *et al.*, 1985; Reynolds, 1985*b*; Cawthorn *et al.*, 2005). This is also the case for our samples, as indicated in the lithological cycle.

Crystal settling and sorting has typically been proposed to explain the magnetitite and chromitite layers (Cawthorn *et al.*, 2005; Bai *et al.*, 2012; Namur *et al.*, 2015) in many layered intrusions. However, the absence of pyroxene, which has an intermediate density between magnetite and plagioclase, leads to a gravity

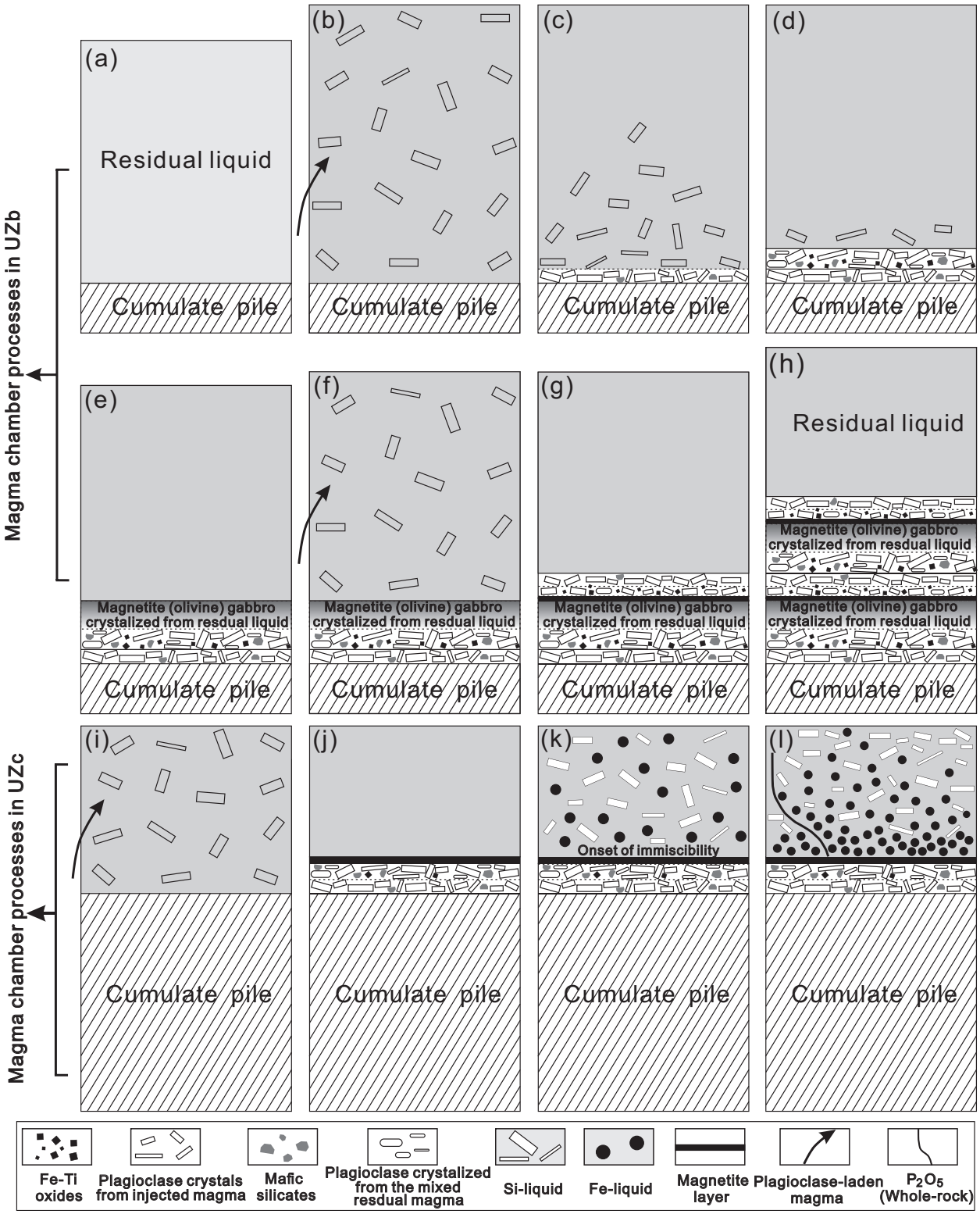

Fig. 15. Schematic illustration of magma chamber processes in the Bushveld Complex, which can account for the typical lithological sequence of anorthosite, pmi-C, magnetite (olivine) gabbro and oxide-rich rocks in UZb, and anorthositic, magnetite layer, nelsonite, magnetite troctolite and magnetite olivine gabbro observed in the phosphorus cycles in UZc.

problem for a sorting mechanism (Cawthorn *et al.*, 2005; Cawthorn & Ashwal, 2009) because the typical Bushveld magma saturated in plagioclase and magnetite is also saturated in pyroxene. The formation of hybrid magmas after mixing with plagioclase-laden magmas can solve this issue and explains the absence of pyroxene above the magnetite layers. We therefore propose that magnetite layers are the result of crystal

settling from the pmi-C saturated magma, which is produced by magma mixing.

Origin of nelsonite in UZc

Silicate liquid immiscibility has been recently identified as a major process of differentiation in the UZ of the Bushveld Complex (VanTongeren & Mathez, 2012; Fischer *et al.*, 2016). Residual liquids reached a two-liquid field upon cooling and produced immiscible silica- and iron-rich melts (Charlier & Grove, 2012), which further crystallized to form cumulate rocks (Namur *et al.*, 2012). The implication of this process for the complete stratigraphy of the UZc is discussed in our study, because of the complete record of bulk-rock chemistry and mineral compositions.

The upper cycles in UZc after apatite saturation are notable for a series of thick magnetite and nelsonite layers and a continuous bottom-up decrease in P_2O_5 in bulk-rock compositions within each cycle. Slightly after the mixing process in the basal reversal, the magnetite layers formed most probably as a result of a similar process to that mentioned above for the magnetite layers in UZa and UZb, followed by a sharp increase in apatite in the nelsonite/troctolite rocks. After that, the content of phosphorus decreases smoothly up section.

A recent study by Fischer *et al.* (2016) of apatite-hosted multiphase inclusions in the same UZc samples as analyzed in this study proved the existence of two silicate liquid end-members, of iron-rich and silica-rich composition, created by an immiscibility process. The segregation of conjugate immiscible melts and their crystallization produced a cumulate pile ranging from melanogabbro (dominated by minerals crystallized from the Fe-rich melt; i.e. apatite and Fe–Ti oxides) to leucogabbro (dominated by plagioclase crystallized from the Si-rich melt) depending on the relative proportions of the two melts. The upward decrease in the proportion of Fe–Ti oxides in these cycles (Supplementary Data Fig. S5b) is explained by the downward percolation of the dense, low-viscosity, iron-rich liquid.

Regarding the implications of immiscibility on the formation of nelsonite layers, we note that the immiscible iron-rich liquids contain a maximum of 40 wt % FeO_{tot} (Jakobsen *et al.*, 2005; Charlier *et al.*, 2011, 2013; Fischer *et al.*, 2016), which cannot account for the 60–70 wt % FeO_{tot} in Fe–Ti–P layers. We rather propose that Fe–Ti–P layers represent the cumulate products of those immiscible melts (Namur *et al.*, 2012).

Synthesis model for the crystallization of the Upper Zone

After magma addition at the PM, the residual magma in the UUMZ chamber progressively evolved on an Fe-enrichment trend. Pulses of plagioclase-laden magmas were emplaced, forming the anorthosite layers at the bottom of each cycle (Fig. 15a–c). Mush emplacement was subsequently followed by magma mixing between the resident magma and the new liquid; the mixing led to a hybrid melt that produced a number of pmi-C rocks (Fig. 15d). After the deposition of these pmi-C rocks, further cooling and differentiation drove the melt to become saturated with pyroxenes and olivine, and magnetite (olivine) gabbronorites crystallized (Fig. 15e). A similar mush emplacement and magma mixing process occurred cyclically and produced the pmi-C liquid. Crystal sorting further led to the formation of the magnetite layer above the magnetite (olivine) gabbronorite (Fig. 15f and g).

In UZc, subsequent to the replenishment of crystal-laden magma, anorthosites formed in the basal part of each cycle (Fig. 15i and j), followed by magnetite layers formed from hybrid magmas similar to those in UZa and UZb. After apatite saturation, immiscibility occurred immediately, preventing the formation of leucogabbros (Fig. 15k) and leading to downward percolation of the dense immiscible iron-rich liquid (Fischer *et al.*, 2016). This resulted in the formation of a layer with a high proportion of Fe–Ti oxides, apatite and olivine, accumulated adjacent to the basal anorthosite, forming nelsonites and magnetite troctolites (Fig. 15l).

Our model relies on new evidence for the close association between magnetite layers and anorthosite layers. The intermediate assemblage of pmi-C rocks documented in UZa and UZb, closely related to the magnetite layers, is a cumulate product formed after mixing of the residual magma with replenished plagioclase-laden magma. This rock type provides a link between the formation of anorthosite and magnetite layers. Our model can explain the progressive upper contact with anorthosite formed during the mush emplacement and the sharp lower contacts with anorthositic rocks (von Gruenewaldt, 1973; Molyneux, 1974). In addition, our model for UZc can also account for the sequence of magnetite, nelsonite, magnetite troctolite and magnetite olivine gabbro layers followed by magnetite-rich rocks in the typical lithological section of the phosphorus cycle (Fig. 13d). Finally, we can clearly identify different mechanisms for formation of magnetitite (magma mixing; this study) and nelsonite layers (immiscibility; Fischer *et al.*, 2016) in the UUMZ, which may also shed light on the Fe–Ti–P layers in other mafic layered intrusions.

CONCLUSIONS

New systematic bulk-rock major and trace element analyses, precise mineral modes determined by FE-SEM scanning and CIPW norms, and microprobe analyses of plagioclase, high-Ca pyroxene, olivine and low-Ca pyroxene, combined with the published Cr contents of magnetite separates from the Bierkraal drill cores from the Upper Main Zone and Upper Zone in the western limb of the Bushveld Complex allow us to reach the following conclusions.

(1) The least evolved liquidus phases of the UUMZ include plagioclase, high-Ca pyroxene and low-Ca pyroxene. Fe–Ti oxides, olivine and finally apatite then appear progressively in the crystallization sequence.

Cumulus K-feldspar, quartz and amphibole also appear in the most evolved part at the top.

(2) Although the samples exhibit a broad fractionation trend, a series of compositional reversals in the anorthite content of plagioclase, Mg# in pyroxenes and olivine, and Cr in magnetite separates and bulk-rocks are observed. Most of these reversals are correlated with the absence of some cumulus minerals (pyroxene, olivine, apatite, Fe–Ti oxides) or the appearance of monomineralic layers. These reversals are used as boundaries to divide the UUMZ into 18 cycles.

(3) Within most of these cycles, anorthosites and leucogabbros are linked with compositional reversals and are interpreted as evidence for magma replenishment with plagioclase-bearing magma. In particular, the abundant pmi-C samples in UZa and UZb are interpreted as having formed from a hybrid melt resulting from the mixing between the resident magma and newly injected plagioclase-bearing magma. The Bushveld UUMZ grew by multiple emplacements of crystal-laden magmas coming from one or several deep-located chamber(s).

(4) In the UZc, mush emplacement also occurred and produced magnetite layers similar to those in UZa and UZb. Soon after the saturation of apatite in UZc, the residual magma reached silicate liquid immiscibility. Segregation of the conjugate Fe-rich and Si-rich melts explains the smooth upward decrease of Fe–Ti oxides and increase of plagioclase proportion in the upper apatite-bearing cycles (XII to XVIII); the crystallization of the Fe-rich magma may account for the nelsonite layers above the magnetite layers.

(5) Our detailed lithological stratigraphy and geochemical comparison with other limbs of the Bushveld intrusion proves that there are many similarities between the western and eastern limbs, but indicates that the Bellevue section of the northern limb has notable differences.

ACKNOWLEDGEMENTS

We appreciate the help of Nicolas Delmelle (University of Liège), Roman Klinghardt (RWTH Aachen University), P. E. Wolff, Renat Almeev, Chao Zhang and Dongmei Qi (Leibniz Universität Hannover) with whole-rock and microprobe analyses, and thank V. D. Kamenetsky, K. Goemann and S. T. Feig from the University of Tasmania for support with the SEM analyses. We also thank Marian Holness and Zoja Vukmanovic for helpful discussions on mineral textures. Comments from Professor J. C. Duchesne were greatly appreciated. We are grateful for reviews by Ed Mathez, Allan Wilson and Sarah-Jane Barnes, which helped to improve the paper significantly. We thank Marjorie Wilson and Alastair Lumsden for their editorial work.

FUNDING

Q. Yuan acknowledges support from China Scholarship Council (201406410015). B. Charlier and O. Namur acknowledge support from the Alexander von Humboldt Foundation. O. Namur also acknowledges support from the DFG through an Emmy Noether program. The project was supported by DFG grant KO 1723/20–1.

SUPPLEMENTARY DATA

Supplementary data for this paper are available at *Journal of Petrology* online.

REFERENCES

Ashwal, L. D., Webb, S. J. & Knoper, M. W. (2005). Magmatic stratigraphy in the Bushveld Northern Lobe: continuous geophysical and mineralogical data from the 2950 m Bellevue drillcore. *South African Journal of Geology* **108**, 199–232.

Bai, Z. J., Zhong, H., Naldrett, A. J., Zhu, W. G. & Xu, G. W. (2012). Whole-rock and mineral composition constraints on the genesis of the giant Hongge Fe–Ti–V oxide deposit in the Emeishan Large Igneous Province, Southwest China. *Economic Geology* **107**, 507–524.

Barnes, S. J. (1986). The effect of trapped liquid crystallization on cumulus mineral compositions in layered intrusions. *Contributions to Mineralogy and Petrology* **93**, 524–531.

Barnes, S.-J. & Maier, W. D. (2002). Platinum-group element distributions in the Rustenberg Layered Suite of the Bushveld Complex, South Africa. In: Cabri, L. J. (ed.) *The Geology, Geochemistry, Mineralogy and Mineral Beneficiation of Platinum-Group Elements. Canadian Institute of Mining, Metallurgy and Petroleum, Special Volume* **54**, 431–458.

Barnes, S.-J., Maier, W. D. & Curl, E. A. (2010). Composition of the marginal rocks and sills of the Rustenburg Layered Suite, Bushveld Complex, South Africa: implications for the formation of the platinum-group element deposits. *Economic Geology* **105**, 1491–1511.

Bédard, J. H. J., Marsh, B. D., Hersum, T. G., Naslund, H. R. & Mukasa, S. B. (2007). Large-scale mechanical redistribution of orthopyroxene and plagioclase in the basement sill, Ferrar dolerites, McMurdo Dry Valleys, Antarctica: Petrological, mineral-chemical and field evidence for channelized movement of crystals and melt. *Journal of Petrology* **48**, 2289–2326.

Buchanan, P. C., Koeberl, C. & Reimold, W. U. (1999). Petrogenesis of the Dullstroom Formation, Bushveld Magmatic Province, South Africa. *Contributions to Mineralogy and Petrology* **137**, 133–146.

Buchanan, P. C., Reimold, W. U., Koeberl, C. & Kruger, F. J. (2002). Geochemistry of intermediate to siliceous volcanic rocks of the Rooiberg Group, Bushveld Magmatic Province, South Africa. *Contributions to Mineralogy and Petrology* **144**, 131–143.

Buchanan, P. C., Reimold, W. U., Koeberl, C. & Kruger, F. J. (2004). Rb–Sr and Sm–Nd isotopic compositions of the Rooiberg Group, South Africa: early Bushveld-related volcanism. *Lithos* **75**, 373–388.

Buick, I. S., Maas, R. & Gibson, R. (2001). Precise U–Pb titanite age constraints on the emplacement of the Bushveld Complex, South Africa. *Journal of the Geological Society, London* **158**, 3–6.

Cawthorn, R. G. (2015). The Bushveld Complex, South Africa. In: Charlier, B., Namur, O., Latypov, R. & Tegner, C. (eds) *Layered Intrusions*. Dordrecht: Springer, pp. 517–587.

Cawthorn, R. G. & Ashwal, L. D. (2009). Origin of anorthosite and magnetitite layers in the Bushveld Complex, constrained by major element compositions of plagioclase. *Journal of Petrology* **50**, 1607–1637.

Cawthorn, R. G. & McCarthy, T. S. (1985). Incompatible trace element behavior in the Bushveld complex. *Economic Geology* **80**, 1016–1026.

Cawthorn, R. G. & Molyneux, T. G. (1986). Vanadiferous magnetite deposits of the Bushveld Complex. In: Anhaeusser, C. R & Maske, S. (eds) *Mineral Deposits of Southern Africa*. Johannesburg: Geological Society of South Africa, pp. 1251–1266.

Cawthorn, R. G. & Walraven, F. (1998). Emplacement and crystallization time for the Bushveld Complex. *Journal of Petrology* **39**, 1669–1687.

Cawthorn, R. G. & Walsh, K. L. (1988). The use of phosphorus contents in yielding estimates of the proportion of trapped liquid in cumulates of the Upper Zone of the Bushveld Complex. *Mineralogical Magazine* **52**, 81–89.

Cawthorn, R. G., Meyer, P. S. & Kruger, F. J. (1991). Major addition of magma at the Pyroxenite Marker in the western Bushveld Complex, South Africa. *Journal of Petrology* **32**, 739–763.

Cawthorn, R. G., Barnes, S. J., Balhaus, C. & Malich, K. N. (2005). Platinum-group element, chromium and vanadium deposits in mafic and ultramafic rocks. *Economic Geology, 100th Anniversary Volume* 215–249.

Cawthorn, R. G., Lundgaard, K. L., Tegner, C. & Wilson, J. R. (2016). Lateral variations in plagioclase compositions, Main Zone, Bushveld Complex, South Africa: Evidence for slow mixing of magmas in basinal structures. *Mineralogical Magazine* **80**, 213–225.

Charlier, B. & Grove, T. L. (2012). Experiments on liquid immiscibility along tholeiitic liquid lines of descent. *Contributions to Mineralogy and Petrology* **164**, 27–44.

Charlier, B., Namur, O., Toplis, M. J., Schiano, P., Cluzel, N., Higgins, M. D. & Vander Auwera, J. (2011). Large-scale silicate liquid immiscibility during differentiation of tholeiitic basalt to granite and the origin of the Daly gap. *Geology* **39**, 907–910.

Charlier, B., Namur, O. & Grove, T. L. (2013). Compositional and kinetic controls on liquid immiscibility in ferrobasalt–rhyolite volcanic and plutonic series. *Geochimica et Cosmochimica Acta* **113**, 79–93.

Czamanske, G. K. & Bohlen, S. R. (1990). The Stillwater Complex and its anorthosites: an accident of magmatic underplating? *American Mineralogist* **75**, 37–45.

Eales, H. V. & Cawthorn, R. G. (1996). The Bushveld Complex. In: Cawthorn, R. G. (ed.) *Layered Intrusions. Developments in Petrology, 15*. Amsterdam: Elsevier, pp. 181–229.

Engelbrecht, J. P. (1985). The chromites of the Bushveld Complex in the Nietverdiend area. *Economic Geology* **80**, 896–910.

Fischer, L. A., Wang, M., Charlier, B., Namur, O., Roberts, R. J., Veksler, I. V, Cawthorn, R. G. & Holtz, F. (2016). Immiscible iron- and silica-rich liquids in the Upper Zone of the Bushveld Complex. *Earth and Planetary Science Letters* **443**, 108–117.

Grove, T. L., Baker, M. B. & Kinzler, R. J. (1984). Coupled CaAl–NaSi diffusion in plagioclase feldspar: experiments and applications to cooling rate speedometry. *Geochimica et Cosmochimica Acta* **48**, 2113–2121.

Hall, A. L. (1932). The Bushveld Igneous Complex in the central Transvaal. *Geological Society of South Africa, Memoir* **28**, 544 pp.

Hayes, B., Ashwal, L. D., Webb, S. J. & Bybee, G. M. (2017). Large-scale magmatic layering in the Main Zone of the Bushveld Complex and episodic downward magma infiltration. *Contributions to Mineralogy and Petrology* **172**, 13.

Irvine, T. N. (1982). Terminology for layered intrusions. *Journal of Petrology* **23**, 127–162.

Jakobsen, J. K., Veksler, I. V., Tegner, C. & Brooks, C. K. (2005). Immiscible iron- and silica-rich melts in basalts petrogenesis documented in the Skaergaard intrusion. *Geology* **33**, 885–888.

Kruger, F. J., Cawthorn, R. G. & Walsh, K. L. (1987). Strontium isotopic evidence against magma addition in the Upper Zone of the Bushveld Complex. *Earth and Planetary Science Letters* **84**, 51–58.

Lee, C. A. (1996). A review of mineralization in the Bushveld Complex and some other layered intrusions. In: Cawthorn, R. G. (ed.) *Layered Intrusions*. Developments in Petrology, 15. Amsterdam: Elsevier, pp. 103–145.

Lum, J. E. (2011). Plagioclase compositions in the Upper Zone of the Bushveld Complex. MS thesis, University of the Witwatersrand, Johannesburg, 184 pp.

Maier, W. D., Barnes, S.-J. & Groves, D. I. (2012). The Bushveld Complex, South Africa: formation of platinum–palladium, chrome- and vanadium-rich layers via hydrodynamic sorting of a mobilized cumulate slurry in a large, relatively slowly cooling, subsiding magma chamber. *Mineralium Deposita* **48**, 1–56.

Maier, W. D., Barnes, S.-J. & Karykowski, B. T. (2016). A chilled margin of komatiite and Mg-rich basaltic andesite in the western Bushveld Complex, South Africa. *Contributions to Mineralogy and Petrology* **171**, 57–79.

Maila, R. P. (2015). Geochemistry of magnetitite layers in the Upper Zone of the Bushveld Complex, South Africa. MS thesis, University of the Witwatersrand, Johannesburg, 128 pp.

Marsh, B. D. (2013). On some fundamentals of igneous petrology. *Contributions to Mineralogy and Petrology* **166**, 665–690.

Mathez, E. A., VanTongeren, J. A. & Schweitzer, J. (2013). On the relationships between the Bushveld Complex and its felsic roof rocks, part 1: Petrogenesis of Rooiberg and related felsites. *Contributions to Mineralogy and Petrology* **166**, 435–449.

McCarthy, T. S., Cawthorn, R. G., Wright, C. J. & McIver, J. R. (1985). Mineral layering in the Bushveld complex: Implications of Cr abundances in magnetite from closely spaced magnetitite and intervening silicate-rich layers. *Economic Geology* **80**, 1062–1074.

Merkle, R. K. W. & von Gruenewaldt, G. (1986). Compositional variation of Co-rich pentlandite: relation to the evolution of the Upper Zone of the Western Bushveld Complex, South Africa. *Canadian Mineralogist* **24**, 529–546.

Mitchell, A. A. (1996). Compositional cyclicity in a pyroxenitic layer from the Main Zone of the Western Bushveld Complex: evidence for repeated magma influx. *Mineralogical Magazine* **60**, 149–161.

Molyneux, T. G. (1974). A geological investigation of the Bushveld Complex in Sekhukhuneland and part of the Steelpoort valley. *Transactions of the Geological Society of South Africa* **77**, 329–338.

Namur, O., Charlier, B., Toplis, M. J., Higgins, M. D., Liégeois, J. P. & Vander Auwera, J. (2010). Crystallization sequence and magma chamber processes in the ferrobasaltic Sept Iles layered intrusion, Canada. *Journal of Petrology* **51**, 1203–1236.

Namur, O., Charlier, B. & Holness, M. (2012). Dual origin of Fe–Ti–P gabbros by immiscibility and fractional crystallization of evolved tholeiitic basalts in the Sept Iles layered intrusion. *Lithos* **154**, 100–114.

Namur, O., Abily, B., Boudreau, A., Blanchette, F., Bush, J. W. M., Ceuleneer, G., Charlier, B., Donaldson, C. H., Higgins, M.

D., Morata, D., Nielsen, T. F. D., O'Driscoll, B., Pang, K. N., Peacock, T., Spandler, C. J., Toramaru, A. & Veksler, I. V. (2015). Igneous layering in basaltic magma chambers. In: Charlier, B., Namur, O., Latypov, R. & Tegner, C. (eds) *Layered Intrusions*. Dordrecht: Springer, pp. 75–152.

Pouchou, J. L. & Pichoir, F. (1991). Quantitative analysis of homogeneous or stratified microvolumes applying the model 'PAP'. *Electron Probe Quantification* **1**, 31–75.

Raedeke, L. D. (1982). Petrogenesis of the Stillwater Complex. PhD thesis, University of Washington, Seattle, 212 pp.

Reynolds, I. M. (1985*a*). The nature and origin of titaniferous magnetite-rich layers in the Upper Zone of the Bushveld Complex: A review and synthesis. *Economic Geology* **80**, 1089–1108.

Reynolds, I. M. (1985*b*). Contrasted mineralogy and textural relationships in the uppermost titaniferous magnetite layers of the Bushveld complex in the Bierkraal area north of Rustenburg. *Economic Geology* **80**, 1027–1048.

Riker, J. M., Cashman, K. V., Rust, A. C. & Blundy, J. D. (2015). Experimental constraints on plagioclase crystallization during H_2O- and H_2O–CO_2-saturated magma decompression. *Journal of Petrology* **56**, 1967–1998.

Roeder, P. L. & Osborn, E. F. (1966). Experimental data for the system MgO–FeO–Fe_2O_3–$CaAl_2Si_2O_8$–SiO_2 and their petrologic implications. *American Journal of Science* **264**, 428–480.

Roelofse, F. & Ashwal, L. D. (2012). The lower Main Zone in the Northern Limb of the Bushveld Complex—a >1·3 km thick sequence of intruded and variably contaminated crystal mushes. *Journal of Petrology* **53**, 1449–1476.

Roelofse, F., Ashwal, L. D. & Romer, R. L. (2015). Multiple, isotopically heterogeneous plagioclase populations in the Bushveld Complex suggest mush intrusion. *Chemie der Erde* **75**, 357–364.

(South African Committee for Stratigraphy) SACS (1980). Lithostratigraphy of the Republic of South Africa, South West Africa/Namibia, and the Republics of Bophuthatswana, Transkei and Venda. In: Kent, L. E. (ed.) *Stratigraphy of South Africa, Part 1*. Geological Survey of South Africa, p. 690.

Scoon, R. N. & Mitchell, A. (2012). The Upper Zone of the Bushveld Complex at Roossenekal, South Africa: geochemical stratigraphy and evidence of multiple episodes of magma replenishment. *South African Journal of Geology* **115**, 515–534.

Scoon, R. N. & Mitchell, A. (2014). Discussion of 'The Bushveld Complex, South Africa: formation of platinum–palladium, chrome- and vanadium-rich layers via hydrodynamic sorting of a mobilized cumulate slurry in a large, relatively slowly cooling, subsiding magma chamber' by Maier et al. (2013) Miner Deposita 48:1–56. *Mineralium Deposita* **49**, 399–404.

Sharpe, M. R. (1985). Strontium isotope evidence for preserved density stratification in the main zone of the Bushveld Complex, South Africa. *Nature* **316**, 119–126.

Tegner, C., Cawthorn, R. G. & Kruger, F. J. (2006). Cyclicity in the Main and Upper Zones of the Bushveld Complex, South Africa: crystallization from a zoned magma sheet. *Journal of Petrology* **47**, 2257–2279.

VanTongeren, J. A. & Mathez, E. A. (2012). Large-scale liquid immiscibility at the top of the Bushveld Complex, South Africa. *Geology* **40**, 491–494.

VanTongeren, J. A. & Mathez, E. A. (2013). Incoming magma composition and style of recharge below the Pyroxenite Marker, Eastern Bushveld Complex, South Africa. *Journal of Petrology* **54**, 1585–1605.

VanTongeren, J. A., Mathez, E. A. & Kelemen, P. B. (2010). A felsic end to Bushveld differentiation. *Journal of Petrology* **51**, 1891–1912.

VanTongeren, J. A., Zirakparvar, N. A. & Mathez, E. A. (2016). Lithos Hf isotopic evidence for a cogenetic magma source for the Bushveld Complex and associated felsic magmas. *Lithos* **248–251**, 469–477.

Vermaak, C. F. (1976). The Merensky Reef—thoughts on its environment and genesis. *Economic Geology* **71**, 1270–1298.

von Gruenewaldt, G. (1973). The Main and Upper zones of the Bushveld Complex in the Roossenekal area, Eastern Transval. *Transactions of the Geological Society of South Africa* **76**, 207–227.

von Gruenewaldt, G. (1993). Ilmenite–apatite enrichments in the Upper Zone of the Bushveld complex: A major titanium–rock phosphate resource. *International Geology Review* **35**, 987–1000.

von Gruenewaldt, G., Klemm, D. D., Henckel, J. & Dehm, R. M. (1985). Exsolution features in titanomagnetites from massive magnetite layers and their host rocks of the Upper Zone, eastern Bushveld complex. *Economic Geology* **80**, 1049–1061.

Wager, L. R. & Brown, G. M. (1968). *Layered Igneous Rocks*. Edinburgh: Oliver & Boyd.

Walraven, F. & Wolmarans, L. G. (1979). Stratigraphy of the upper part of the Rustenburg Layered Suite, Bushveld complex, in the western Transvaal. *Annals of the Geological Survey of South Africa* **13**, 109–114.

Webb, S. J., Ashwal, L. D. & Cawthorn, R. G. (2011). Continuity between eastern and western Bushveld Complex, confirmed by xenoliths from kimberlite. *Contributions to Mineralogy and Petrology* **162**, 101–107.

Willemse, J. (1969*a*). The vanadiferous magnetic iron ore of the Bushveld Igneous Complex. *Economic Geology Monograph* **4**, 187–208.

Willemse, J. (1969*b*). The geology of the Bushveld Igneous Complex, the largest repository of magmatic ore deposits in the world. *Economic Geology Monograph* **4**, 1–22.

Wilson, A. H. (2012). A chill sequence to the Bushveld Complex: Insight into the first stage of emplacement and implications for the parental magmas. *Journal of Petrology* **53**, 1123–1168.

Wilson, A. H. (2015). The earliest stages of emplacement of the Eastern Bushveld Complex: development of the Lower Zone, Marginal Zone and Basal ultramafic sequence. *Journal of Petrology* **56**, 347–388.

Wilson, J. R. & Sorensen, H. S. (1996). The Fongen–Hyllingen layered intrusive complex, Norway. In: Cawthorn, R. G. (ed.) *Layered Intrusions*. Developments in Petrology, 15. Amsterdam; Elsevier, pp. 303–329.

Zeh, A., Ovtcharova, M., Wilson, A. H. & Schaltegger, U. (2015). The Bushveld Complex was emplaced and cooled in less than one million years—results of zirconology, and geotectonic implications. *Earth and Planetary Science Letters* **418**, 103–114.